Performance modeling of MED-MVC systems: exergy-economic analysis.

Mohamed L. Elsayed [a,b,1], Osama Mesalhy [a,b], Ramy H. Mohammed [a,b], Louis C. Chow [a]
[a]Department of Mechanical and Aerospace Engineering, University of Central Florida, Orlando, FL 32816-2450, USA.
[b]Department of Mechanical Power Engineering, Zagazig University, Zagazig 44519, Egypt.

ABSTRACT

In this study, exergy analysis of four different feed configurations of a multi-effect desalination with mechanical vapor compressor (MED-MVC) system is initially studied to identify the area of exergy destruction within system components and followed by an exergo-economic study. The feed configurations considered are forward feed (FF), backward feed (BF), parallel feed (PF) and parallel/cross feed (PCF). From the 1st law energy analysis, the PCF and FF configurations require less work to achieve equal distillate production compared to other two configurations. For instance, the specific power consumption (SPC) values are 30.1, 13.7, 23 and 13.9 kWh/m^3 for the BF, FF, PF and PCF configurations, respectively. Changing the feed arrangement from BF to FF and PF to PCF at a constant compression ratio, the total fixed cost for the MED-MVC plant can be reduced by ~30% and 17%, respectively. Second law efficiency (η_{II}) calculations show that the PCF (2.9%) has the highest value followed by the FF (2.7%), while the BF (2.4%) exhibits the lowest value among all configurations. The highest exergy destruction (35-50%) occurs within the MVC unit. This can be reduced by limiting the design plant operation to a lower temperature range or increasing the number of effects. Increasing the number of effects for PCF from 1 to 6 results in a 39% reduction in the SPC and a 70% increase in the second law efficiency. Operating at lower steam temperature results in an increase in the $\eta_{II,}$and a decrease in the SPC and total water price (TWP) of the MED-MVC system. Reducing the exergy destruction in the preheaters and the MVC unit is cost-effective for the entire system even with an increase in capital investment costs. Three different cost models are used to estimate the average TWPs for the BF, FF, PF and PCF configurations, and the TWPs are found to be 3.0, 1.7, 2.4 and 1.7 \$/m^3, respectively.

KEYWORDS: Exergo-economic; water price; Mechanical vapor compression (MVC); Cost flow diagram.

1. Introduction

Multi-effect desalination with mechanical vapor compressor (MED-MVC) systems are widely applied as a common solution for medium-scale (100-5000 m^3/day) water reclamation desalination and solution

[1]Corresponding author, e-mail address: mlea@knights.ucf.edu, mlabdelkrem@zu.edu.eg (Mohamed L. Elsayed).

concentration for high-salinity wastewater treatment (salt recovery) [1]. Several advantages associated with MVC systems include high-quality water recovered, compact equipment, low-temperature design and long-term stable operation. Corrosion and scale formation are minimal which lead to high plant operation availabilities [2, 3]. The main limitation of the MED-MVC systems is the low capacity of the available mechanical vapor compressors (MVC). The low volumetric flow and pressure head limit the production capacity to 5000 m^3/day [4]. The MVC units are typically radial centrifugal or axial flow compressors due to their high suction flow rates and low maintenance requirements and could be single stage or multistage with intercoolers [5, 6].

Various studies for MVC systems available in the literature include steady-state model development, simplified design methods, experimental research and performance prediction. Some of these studies, as well as a few others of interest, are presented in the following paragraphs. There are more experimental studies on the MVC systems than theoretical investigations [7]. For example, Veza [8] and Lucas and Tabourier [9] described a MVC seawater desalination unit producing 500 and 1500 m^3/day of distilled water at a specific power consumption (SPC) of 11.5 and 11 kWh/m^3, respectively when operating at 40% water recovery. Bahar [10] tested a MVC pilot plant with two vertical double fluted tubes evaporators with one m^3/day capacity and a top brine temperature (TBT) of 103°C. The highest performance ratio (ratio of kg of distillate output to 2326 kJ of heat input) obtained was 2.52. A single-effect MVC system with a 5 m^3/day capacity was experimentally tested by Aly and Fiqi [11] with mathematical modeling included. Two immersion electrical heaters were used to provide the steam needed to start the desalination process. The amount of steam was based on the supplied feed seawater temperature and the compressor power. There were several efforts made to operate MVC systems with renewable energy resources, since they are more tolerant to intermittent operation compared to the reverse osmosis (RO) process. For instance, Plantikow [12] presented a wind-powered MVC desalination plant installed in Germany which was capable of producing 360 m^3/day of freshwater with a SPC of 16.7 kWh/m^3.

The process performance of MVC units varies slightly, depending on the application. Beyond seawater treatment, MVC has been used to produce water from heavy oil fields and high salinity wastewater treatment in recent years. The MVC process presents some advantages compared to other technologies [13]. In crude oil production, the oil in the high-salinity mixture is separated from the water to produce a highly viscous crude through a single-effect MVC with a fresh water capacity of 600 m^3/day at a SPC of 13.6 kWh/m^3 of distillate [14]. To improve the environmental performance and save energy, MVC systems are used as zero-emission desalination (ZED) systems. Han et al. [15] proposed ZED based on a MVC model and showed that the multi-effect ZEDS design is beneficial to reduce the required compressor power compared to the single-effect system. To achieve a salt crystallization concentration of 28.9% from the initial salt mass concentration of seawater of 3%, the required compression work was 760.8 and 604 kJ/kg for single stage and three stages, respectively. Wu et al. [16] presented a novel MVC system with a capacity rated at 1.44 m^3/day. This MVC system separates the evaporator and condenser to overcome the traditional MVC deficiencies such as descaling, anti-scaling and heat transfer conditions for sewage water treatment. Shen et al. [17, 18] revealed that an injection of 5% or less mass fraction of water in a twin-screw compressor with high isentropic efficiency and high-pressure ratio could substantially reduce the SPC, but they recommended its use only for a capacity less than 600 m^3/day. The commercial and experimental pilot plants found in the literature for different applications are shown in Fig. 1 and tabulated in Appendix A, showing the SPC, total water price (TWP) and heat source temperature. For single effect, the SPC has various values which are the highest for desalting of wastewater, oil recovery, and crystallization while in desalination it is in the moderate range.

Steady-state mathematical models of the MVC system are found in many studies. For instance, Aybar [19] and Aussenac et al. [20] developed a model of a single-effect MVC system and analyzed the system performance with variations in the primary parameters. Aly [21] analyzed and compared MVC systems with single, two and three effects. Their results showed that the TWP and the SPC range between 1.3 to 1.7

$/m^3 and 8 to 24 kWh/m^3, respectively. Nafey et al. [22] showed that the MED-MVC system performance decreased by 8% if external steam is used to initiate the evaporation compared to the MVC without external steam. A single-effect MVC for brine crystallization coupled with a wind farm was investigated by Fernández-López [23]. The total capacity is 2400 m^3/day and the SPC is 30.31 kWh/m^3. Helal and Al-Malek [24] presented a hybrid diesel/solar photovoltaic (PV) assisted MVC desalination system. The system was to supply small communities in remote areas with drinkable water at a production capacity of 120 m^3/day. A diesel engine was used to overcome the uncertainty in the availability of solar energy. Henderson et al. [25] proposed a wind/diesel hybrid driven MVC desalination system for off electric grid locations in the USA. Optimization of a similar plant driven by wind/PV hybrid has been carried out by Zejli et al. [26] for a water production capacity of 120 m^3/day. Mounir et al. [27] presented the effect of the temperature difference across the effect on the system cost of a MVC used in pollutant concentration. The results showed that the optimum cost is when the temperature difference is between 2 and 3^{o}C.

Exergy analysis studies are utilized to identify the components with the highest thermodynamic irreversibility rate [28]. For example, Alasfour and Abdulrahim [29] applied steady-state model based on the second law of thermodynamics on a single stage MVC unit. They found that if the temperature difference across the effect increases, the exergy destruction of the unit increases. Nafey et al. [22] analyzed a MED-MVC system with a two-effect forward feed configuration and showed that the plant SPC, second law exergetic efficiency (η_{II}) and the unit product cost are 9.4 kWh/m^3, 5.7% and 1.7 $/m3, respectively. Ahmadi et al. [7] compared single and double effect mechanical vapor recompression (MVR) and showed that energy saving is achieved by using the double-effect MVR instead of the single-effect. Recently, Jamil and Zubair [30] presented an exergo-economic analysis for a MED-MVC system with a forward feed configuration. The second law efficiency, SPC and product cost range from 7 to 10.96%, 7.67 to 11.36 kWh/m^3 and 0.862 to 1.186 $/m^3, respectively when the number of evaporation effects increases from 2 to 6. Their results showed that the percentage of exergy destruction in the MVC unit ranges from 0.03 to

0.05% which is far lower compared to available data in the literature [7, 29, 31, 32]. Moreover, the calculated TWP in their study was much lower than the values reported in the literature [8, 21, 22, 33].

Although there have been many simple modeling studies on the steady-state nature of single-effect MVC [29, 34, 35], there have been little or no adequate contributions on the process design, performance analysis, and economic studies when different feed configurations of MED systems are integrated to a MVC unit. Thus, a comprehensive thermo-economic study of the MED-MVC process is carried out and described in this paper to provide a thorough understanding of the performance of different MED-MVC feed configurations. Steady-state energy and exergo-economic models for different feed configurations of MED-MVC process are used to identify the advantages and deficiencies in each configuration. Three different cost methods (simple conventional economic model, exergy-based component cost model and exergy aggregation model) are used to compare the final price of the freshwater production. The exergo-economic cost model is used to identify the cost concentrated components besides the highest cost flow streams in the system. A sensitivity analysis is conducted to study the impact of the number of effects on the system's performance including the SPC, second law efficiency and TWP. The effects of varying the economic parameters such as cost index factor (C_{index}), interest rate (i) and electricity cost (C_e) on the TWP for different feed configurations of MED-MVC system are investigated as well.

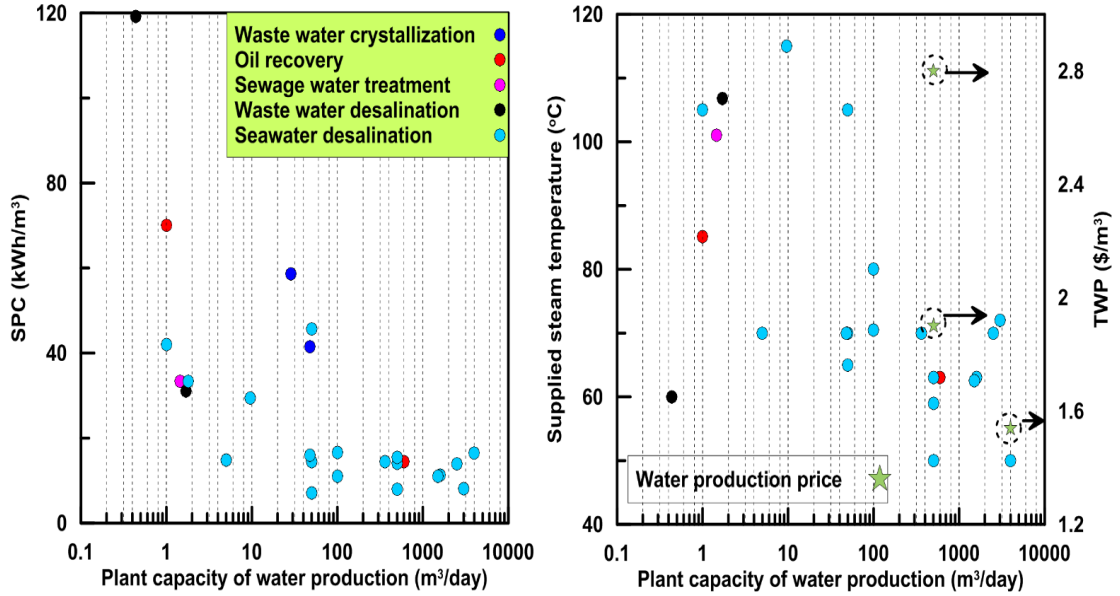

Fig. 1 The influence MVC plant application on the SPC, TWP and steam supplied temperature.

2. Configuration of MED-MVC

Mechanical vapor compression in a MED is a cyclic process. The entire vapor generated in the last effect is routed to the MVC unit through a wire mesh mist eliminator (demister) to separate water droplets from the vapor. The vapor is compressed to the desired target condition of temperature and pressure before directing it as supply steam to the inside of the first effect tubes bundles. The supply steam from the MVC unit condenses to distillate on the tube-side of the first effect by transferring its latent heat to a thin film of feed seawater sprayed around the tubes. A fraction of the sprayed feed evaporates and flows as a heat source to the tubes of the second effect which is at a lower pressure and temperature than the first effect. In MVC desalination systems, the end condenser in a conventional MED is absent as the entire vapor produced in the end effect is sucked out by the mechanical compressor, where it is compressed to increase its enthalpy and used as a heating vapor for supplied feed.

In a MED-MVC, two multi-flow plate-type heat exchangers (pre-heaters) are needed to recuperate the heat coming from both the fresh water product and brine blowdown streams. The product and concentrated brine are drawn off the preheaters by pumps at a temperature slightly above the ambient seawater temperature. Cooling seawater is split up into two portions, and its temperature is elevated to the feed temperature by passing through the pre-heaters and then directed to the MED. Usually, MED-MVC systems are installed where electrical power for operation is available from the grid or through wind energy or other sources of renewable energy. However, for start-up purpose and maintaining standard operating conditions without compressor surges, external steam (make-up steam) extracted from a steam boiler or a power plant steam turbine is used to raise the 1st effect temperature to the TBT [9, 11]. The mechanical energy required for the vapor compressor can be shaft driven if such power is available in a steam power plant. Also, a MVC can be driven with power provided from the electricity grid, wind power plant, geothermal power plant [36], photovoltaic modules or electric generators if electricity services are not available [26]. The MED-MVC system is suitable for use in remote off-public electric grid locations in which water transport is expensive

[12]. This energy is used to activate the MVC unit, pumps, vacuum system and any other control components. It is worth noting that the MVC unit represents the central power consuming component in a MED-MVC system. The power required depends on the pressure difference, on the thermodynamic efficiency of the polytropic process and the efficiency of the electric motor [29, 37].

Multi-effect desalination systems may be represented as some streams exchanging thermal energy among them for achieving the required evaporation [38]. Different configurations differ in the flow directions of the heating steam and the evaporating feed/concentrate or feed water supply. These configurations include forward feed (FF), parallel feed (PF), backward feed (BF) and parallel/cross feed (PCF). Schematic diagrams of different MED configurations are shown in Fig. 2. In each configuration, MVC provides high-temperature steam that enters the tubes side of the first effect as a heating medium to heat and evaporate the feed seawater/brine. In the BF configuration, the entire seawater feed passing through the preheaters is directed to the last effect where it is sprayed onto the tubes, forming a thin liquid film that exchanges heat with the vapor from the previous effect. Part of the feed is evaporated while the temperature and concentration of the remaining portion increase, forming concentrated brine leaving the last effect. In the BF, both seawater feed and steam/vapor have counter-current flow directions. The brine is consecutively cascaded in backward direction through the effects till it approaches the first effect as a feed. In the FF, the entire seawater feed is supplied to the first effect at the highest TBT. The unevaporated brine with high TBT is consecutively cascaded in the forward direction (co-current with the steam/vapor flow) towards the last effect. In the PF, the preheated feed is distributed to all the evaporator effects at the same time. The feed stream to the first effect exchanges heat with the heat source steam and forms brine while the other feed streams exchange heat with the vapor from the previous effects. Here the brine extracted from each effect is at relatively high temperature, so it is directly rejected back to the sea after exchanging heat with the cooling seawater in the brine pre-heater. In the PCF configuration, brine from the first effect is directed to the following effect to utilize its energy by flashing due to an abrupt decrease in pressure. The brine flow process continues to the last effect as shown in Fig. 2.

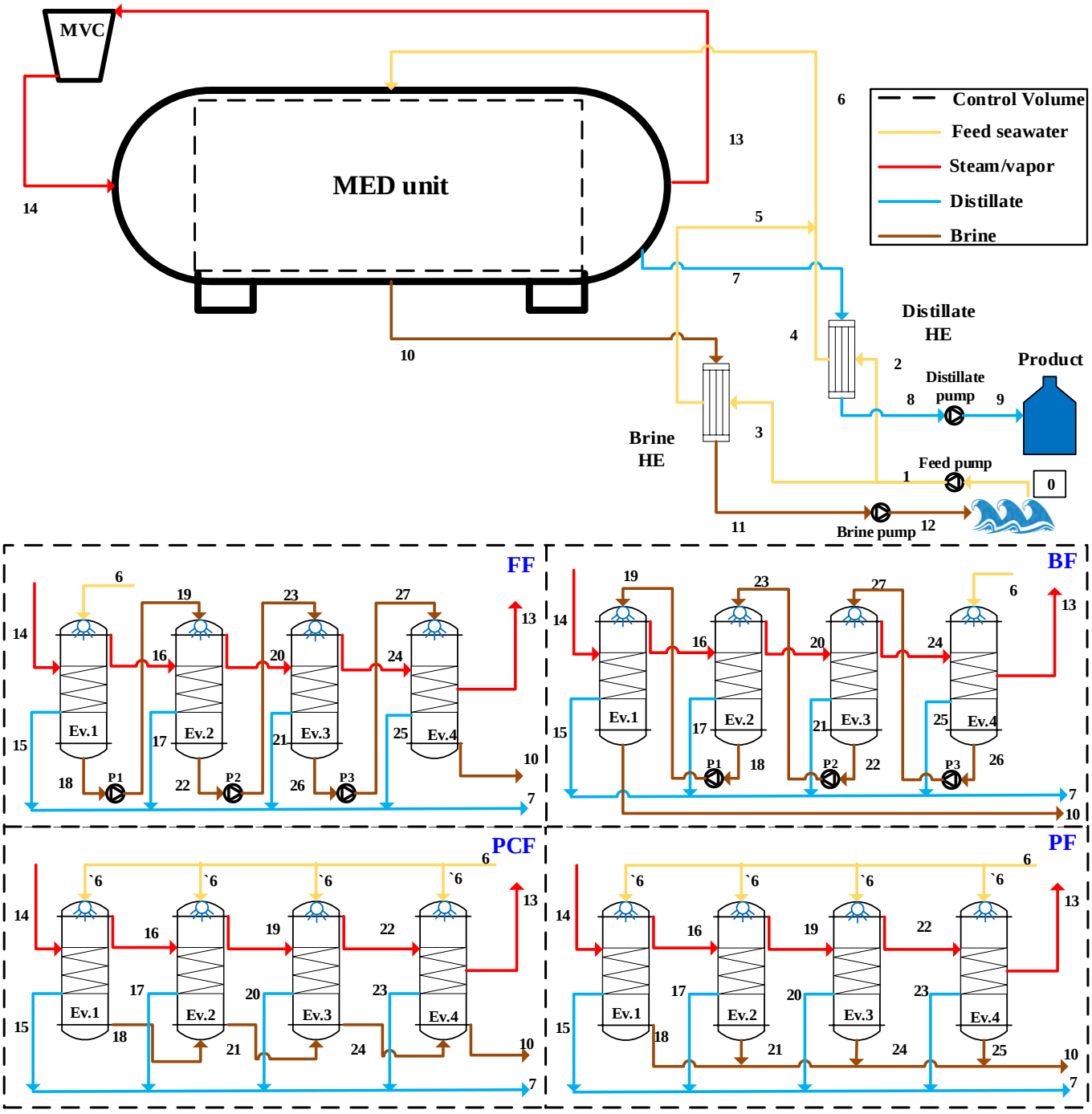

Fig. 2 Flow path of different feed configurations of MED-MVC desalination system.

3. MVC system mathematical model

a. Energy and Exergy modeling

In this study, the steady-state operation of MED-MVC system of different feed arrangements is analyzed to pinpoint the most favorable feed arrangement from the viewpoint of exergo-economic operation. The steady-state conservation equations are solved, and iterative solution method is used to adjust the compressor power

that is required to drive the evaporation process in the first effect. The steady state flow rates of the feed, brine and vapor for each evaporator effect are calculated in addition to the heat transfer surface area and brine salinity. The assumptions used to develop the steady-state model for MED-MVC system are as follows:

1. Thermophysical properties for the brine and vapor are temperature and salinity dependent. Appropriate correlations are selected from [39].
2. Temperature losses between the brine pool and vapor in the effect are; (i) Boiling Point Elevation (BPE), (ii) non-equilibrium allowance (NEA) [39].
3. The vapor and distillate are salt-free [40].
4. Pressure losses of vapor in the connections are ignored.

The mass, energy, and salt balance for BF, FF, PF, and PCF are shown in Table 1. The primary contributor to the power consumption for a MED-MVC system is the power required for the compressor which is a function of inlet vapor specific volume, compression ratio and isentropic compressor efficiency. The secondary consumptions are due to liquid pumps, vacuum pumps and steam boiler during startup [8]. Due to the fixed production capacity of different feed configurations, the amount of vapor in the last effect changes. To ensure balance in all conservation equations, the required thermal energy for the first effect is compensated by the equivalent electricity consumption from the MVC unit. As shown in Fig. 3, the energy supplied to the first effect is defined as:

$$Q_{s,1} = \dot{m}_s . \lambda_s + E_{SH} \quad (1)$$

where $\dot{m}_s \lambda_s$ represents the heat of condensation at T_s of the vapor generated in the last effect and E_{SH} represents enthalpy gained by compression above the energy at saturation condition. The enthalpy of the compressed superheated vapor at the compressor exit ($h_{v,T_s'}$) is expressed in terms of the saturation enthalpy of the compressed vapor (h_{v,T_s}), and enthalpy gained by compression as shown in Fig. 3b:

$$h_{v,T_s'} = h_{v,T_s} + E_{SH}/\dot{m}_s \quad (2)$$

Hence, the actual compressor work can be calculated from:

$$\dot{W}_c = \dot{m}_s.\left(h_{v,T_s} - h_{v,T_n}\right) \tag{3}$$

where, h_{v,T_n} is the saturated vapor enthalpy at the compressor inlet.

Specific power consumption due to the MVC unit and the installed pumps are calculated from:

$$\text{SPC}(kWh/\text{m}^3) = \frac{\dot{W}_{\text{compressor}} + \sum \dot{W}_{\text{pumps}}}{\text{D } (\text{m}^3/h)} \tag{4}$$

The performance ratio (PR) is calculated by the following relation suggested by Nafey [22] which was modified to accommodate the actual work converted to the primary fuel energy [41].

$$\text{PR} = \frac{D\lambda_{distillate}}{\dot{m}_{steam}.\lambda_s + \frac{\dot{W}_{\text{compressor}}}{\eta_{thermal}=0.35}} \tag{5}$$

Two multi-flow direction plate type heat exchangers with effectiveness $\varepsilon = 0.8$ are used in the current simulation to preheat seawater inlet feed by recuperating thermal energy from the distillate and the rejected brine from the MED system. The total feed is divided into two portions to flow in both the brine and distillate heat exchangers. All streams are assumed to be in a liquid phase. The heat transfer area for each heat exchanger can be calculated as follows:

$$A_{HEx} = \frac{\dot{m}_{B,D}\left(h_{10,7} - h_{11,8}\right)}{U_{B,D}.LMTD_{HEx(B,D)}} \tag{6}$$

where h is the enthalpy of the flow stream at a specified temperature as shown in Fig. 2. The log mean temperature differences in the brine and distillate preheaters $LMTD_{HEx(B,D)}$ are evaluated by using the following equation:

$$LMTD_{HEx(B,D)} = \frac{\left(T_{10,7} - T_{5,4}\right) - \left(T_{11,8} - T_{cw}\right)}{ln\left[\frac{T_{10,7} - T_{5,4}}{T_{11,8} - T_{cw}}\right]} \tag{7}$$

The overall heat transfer coefficient for the plate type heat exchangers is calculated by using:

$$U_{B,D} = \left[\frac{1}{h_o} + \frac{1}{h_o} + R_{f,o} + R_{f,o} + \frac{\delta_{plate}}{K_{wall}}\right]^{-1} \quad (8)$$

where K_{wall} is the thermal conductivity of the stainless steel plates, and the inner/outer convective heat transfer coefficients (h_i, h_o) are calculated by using the following correlations [42]:

$$h_{o,i} = 0.2536 Re^{0.65} Pr^{0.4} \left(\frac{K_{wall}}{D_{eq}}\right), Re = \frac{\rho V D_{eq}}{\mu}, D_{eq} = \frac{4(w.t_{plate})}{2(w+t_{plate})} \sim 2t_{plate} \quad (9)$$

where w is the plate width, δ_{plate} is the plate thickness and t_{plate} is the plate spacing. The velocity of each stream is V(m/s) and Re is the stream flow Reynolds number.

As shown in Fig. 3a, the solution procedure starts by assuming the brine temperature in all effects and the energy supplied to the first effect. Then, the equations in Table 1 are solved to determine the feed and brine flow rates as well as the vapor generated in each effect. The mass flow rate imbalance between the vapor generated in the last effect and the required steam for the first effect is minimized iteratively by modifying the term, E_{SH}. This calculation continues till a satisfactory specified accuracy criterion is achieved (ε=10^{-4}). The mixing temperature of the brine and distillate is used to calculate the actual feed temperature by solving the equations of the brine and distillate feed preheaters. The whole calculations are repeated till the specified feed temperature is reached.

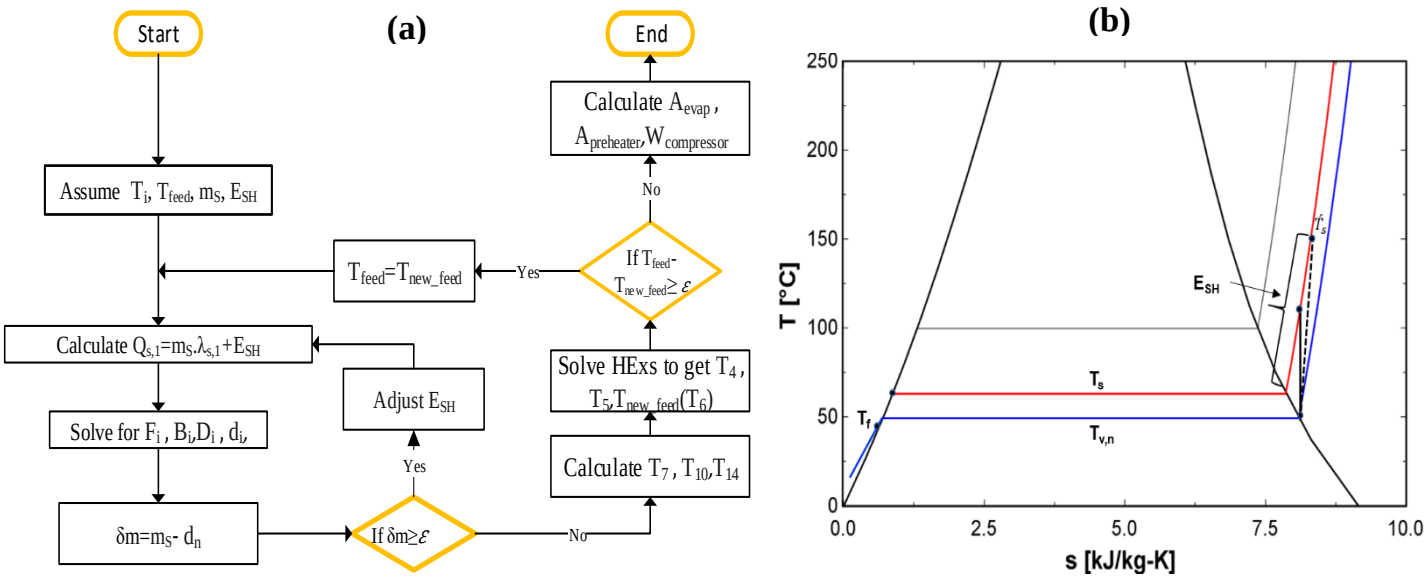

Fig. 3 (a) Flow chart for solution for the steady state model, (b) T-S diagram for MED-MVC system operation.

Table 1 Steady-state balance equations for different feed configurations of MED-MVC system.

Configurations /Equations		First effect	Second to n-1	Last effect (n)	F	B	D
BF	Mass	$B_i = B_{i+1} - D_i$		$B_i = F - D_i$	F_n	B_1	$\sum_{i=1}^{n} D_i$
	Salt	$B_i.X_i = B_{i+1}.X_{i+1}$		$B_i.X_i = F.X_f$			
	Energy	$D_1 = \frac{Q_{s,1} - B_1(h_1 - h_2)}{(\lambda_1 + (h_1 - h_2))}$	$D_i = \frac{D_{i-1}.\lambda_{i-1} - B_i(h_i - h_{i+1})}{(\lambda_1 + (h_i - h_{i+1}))}$	$D_i = \frac{D_{i-1}.\lambda_{i-1} - B_i(h_i - h_f)}{(\lambda_i + (h_i - h_f))}$			
FF	Mass	$B_1 = F - D_1$	$B_i = B_{i-1} - (D_i + d_i)$		F_1	B_n	$\sum_{i=1}^{n} D_i + d_i$
	Salt	$F.X_f = B_1.X_1$	$B_i.X_i = B_{i-1}.X_{i-1}$				
	Energy	$D_1 = \frac{Q_{s,1} - F(h_1 - h_f)}{\lambda_1}$, $d_1 = 0$	$D_i = \frac{(D_{i-1} + d_{i-1}).\lambda_{i-1}}{\lambda_i}$, $d_i = \frac{B_{i-1}(h_{i-1} - h_i)}{\lambda_i}$				
PF	Mass	$B_1 = F_1 - D_1$	$B_i = F_i - D_i$		$\sum_{i=1}^{n} F_i$	$\sum_{i=1}^{n} B_i$	$\sum_{i=1}^{n} D_i$
	Salt	$F_1.X_f = B_1.X_1$	$B_i.X_i = F_i.X_f$				
	Energy	$D_1 = \frac{Q_{s,1} - F_1(h_1 - h_f)}{(\lambda_1)}$	$D_i = \frac{D_{i-1}.\lambda_{i-1}}{\lambda_i} - \frac{F_i(h_i - h_f)}{\lambda_i}$				
PCF	Mass	$B_1 = F_1 - D_1$	$B_i = F_i - D_i + B_{i-1} - d_i$		$\sum_{i=1}^{n} F_i$	B_n	$\sum_{i=1}^{n} D_i + d_i$
	Salt	$F_1.X_f = B_1.X_1$	$B_i.X_i = B_{i-1}.X_{i-1} + F_i.X_f$				
	Energy	$D_1 = \frac{Q_{s,1} - F_1(h_1 - h_f)}{\lambda_1}$, $d_1 = 0$	$D_i = \frac{(D_{i-1} + d_{i-1}).\lambda_{i-1}}{\lambda_i} - \frac{F_i(h_i - h_f)}{\lambda_i}$, $d_i = \frac{B_{i-1}(h_{i-1} - h_i)}{\lambda_i}$				

Total mass balance $F = B + D$

Total salt balance $F.X_f = B.X_n$

d_i , Vapor produced by brine flashing.

D, Total distillate flow rate.

F, Total feed flow rate.

B, Total brine flow rate.

The exergy is known as the maximum available work obtainable when a stream of substance is brought from its initial state to the environmental state. Energy is conserved in any process according to the first law of thermodynamics, but exergy is destroyed due to irreversibilities taking place in entropy creation [43]. For an open system operating under steady state condition, the appropriate exergy rate balance is established including the loss of exergy or loss of work in the following form:

$$\sum_j \left(1 - \frac{T_o}{T_j}\right) \dot{Q}_i + \sum_i \dot{m}_i \, e_i - \sum_e \dot{m}_e \, e_e - \dot{W} - \dot{E}_D = 0 \tag{10}$$

where, $\dot{E}_D$ (kW) is the exergy destruction of the system. The specific exergy transfer terms e_i and e_e can be expressed as the summation of physical, chemical, potential and kinetic exergy [28]. The last two terms are neglected in the current simulation, so the flow exergy takes the following form,

$$e = \overbrace{h - h^* - T_o(s - s^*)}^{physical} + \underbrace{\sum_{i=1}^{n} x_i(\mu_i^* - \mu_i^o)}_{chemical} \tag{11}$$

where h, s, x and μ are specific enthalpy, specific entropy, salt mass fraction and chemical potential, respectively; subscript i represents the species in the mixture; superscript 'o' is for the ambient conditions; and superscript '*' is for the ambient pressure and temperature, and initial concentration of the system conditions. The second law exergetic efficiency for the MED-MVC systems is the ratio of the minimum exergy input required (which is equivalent to the minimum work of separation) to the total actual exergy input. Second law efficiency is used as a criterion of system performance and is calculated considering the exergy loss from the process to the environment as:

$$\eta_{II} = 1 - \frac{\dot{E}_{D,total}}{\dot{E}_{in,total}} = \frac{\dot{W}_{min}}{\dot{E}_{in,total}} \tag{12}$$

where, $\dot{E}_{in,total}$ is the total exergy at the various inlet fluid streams and work provided to the compressor and installed pumps; and $\dot{W}_{min}$ is the minimum work input for the separation of a certain amount of seawater feed at 25°C, 1 atm and a salinity of 36 ppt into fresh water with zero salinity and the rejection of a certain

amount of saline water at the same temperature and pressure. The minimum work is equal to the difference between the exergies of the outgoing and incoming streams as well as the exergy difference due to salinity change. The exergy of the supplied feed seawater is approximately zero as its state is considered as the reference state for exergy calculations [44].

$$\dot{W}_{min} = \dot{E}_9 + \dot{E}_{12} - \dot{E}_0 \quad (13)$$

The exergy analysis is more revealing when the analysis is performed at the component level of different MED-MVC feed configurations. The sites of maximum exergy destruction can be identified. Also, the fraction of exergy destruction within the components is determined to quantify the percentage of exergy destruction in all components for different feed configurations. The exergy balance equation for each component is discussed in detail in the exergo-economic section.

b. Economic models

i. Simple model

The production cost is divided into the direct/indirect cost and annual operating cost. The direct capital cost (DCC) represents the expenses that are directly associated with the construction of the MED plant and the equipment purchasing expenses [45]. Table 2 presents the existing equations in the literature that are used to determine the purchase price of the MED-MVC system components. The other direct cost (land, well construction, auxiliary equipment and building construction) is calculated from [46] for the fixed capacity of 1500 m^3/day to be ~ 80k $. The DCC is equal to the summation of the purchased equipment for the MED-MVC system in Table 2 plus the other costs. Also, the indirect capital cost (freight, insurance, construction overhead, owner's costs and contingency costs) is expressed as a percentage of the total direct capital cost and is assumed as ID_{CC}=0.15DCC [46].

Table 2 Purchase cost of MED-MVC system components.

Instrument	Capital cost of instrument (Z_k) ($)	Comments					Ref.
Preheater (heat exchanger)	$\mathbf{Z_{preheater} = 1000(12.82 + A_{Hex}^{0.8})}$	S for shell side and t for tube side $\boldsymbol{dp}$ (kPa), A (m^2), $\boldsymbol{U}$ $(\boldsymbol{kW/m^2.k})$					[47]
MED effect (evaporator)	$\mathbf{Z_{effect} = 250.26 \times UA_{evaporator} dp_t^{-0.01} dp_s^{-0.1}}$						[48]
Water pump	$\mathbf{Z_{pump} = 13.92 \times \dot{m}_{water}^{0.55} \Delta P^{0.55} \left(\frac{\eta_p}{1-\eta_p}\right)^{1.05}}$	$\boldsymbol{\eta_p = 0.9}$, $\boldsymbol{\Delta P}$ $(\boldsymbol{kPa})$					
			BF	FF	PF	PCF	
		Number of pumps	6	6	3	3	
Compressor (MVC)	$\mathbf{Z_{MVC} = 794.68 \times \dot{W}_{compressor} + 66.11}$	$\dot{\boldsymbol{W}}_{\boldsymbol{compressor}}$ (Watt)					[46]
Other direct costs	$\mathbf{Z_{rest} = 21635.4 \times D^{0.1773}}$	$\boldsymbol{D}$ (m^3/day)					

The operating cost includes all expenses needed after plant commissioning and during plant operation. These expenses can be categorized as variable and fixed costs. The variable operating expenses are those related to the purchase of electrical power, heating steam, chemicals for pre/post-treatment and other requirements that are dependent on the plant capacity of fresh water production and standards. The fixed operating costs represent expenses that are needed for the operation of the plant but are independent of the plant capacity. In many cases, these costs are related to the designed capacity of the plant or taken as a factor of the direct capital cost (DCC). A cost index C_{index} =1.2 is used to accommodate the equipment price change to fit the current reference year calculations. A linearly dependent correlation for the compressor cost of the compressor power is used based on the work done by Lukic et al. [46]. Both operating cost categories are determined based on published data from the literature [39] with maintenance costs taken as a proper subset of the fixed operating cost. Investment and operating & maintenance costs analyses are performed for each configuration using an interest rate set at 5%. The annualized cost method is used to estimate the annual capital cost of system components in this study for 20 years plant lifetime and plant maintenance factor (ϕ) of 1.06. Table 3 illustrates the equations used to calculate the annual capital and operating costs using the amortization cost.

Table 3 Cost parameters for MED desalination plant.

Parameter	Equation	Comments	Ref.
Capital recovery factor, 1/y	$\boldsymbol{CRF = \frac{i.(1+i)^{nt}}{(1+i)^{nt}-1}}$	i is the interest rate 5%, nt (20 year)	[49]
Annual fixed charges, $/y	$\boldsymbol{AFC = (1.38 \times DCC) \times CRF}$		[39]
Annual electric power cost, $/y	$\boldsymbol{AEPC = C_e \times SPC \times \phi \times D \times 365}$	Specific electricity cost $\boldsymbol{C_e = 0.08\ \frac{\$}{kWh}}$	
Annual chemical cost, $/y	$\boldsymbol{ACC = SCC \times \phi \times D \times 365}$	Specific chemical cost $\boldsymbol{SCC = 0.025\ \frac{\$}{m^3}}$	
Annual labor cost, $/y	$\boldsymbol{ALC = SLC \times \phi \times D \times 365}$	Specific labor cost $\boldsymbol{SLC = 0.1\ \frac{\$}{m^3}}$	
Operating and maintenance annual cost, $	$\boldsymbol{OMC = 0.02 \times CRF \times DCC}$		
Total annual cost, $/y	$\boldsymbol{TAC = AFC + AEPC + ACC + ALC + OMC}$		
Total water price $/m^3	$\boldsymbol{TWP_{simple} = \frac{TAC.\phi}{D \times 365}}$		

ii. Exergy-economic model

In the estimation and cost analysis of an energy system, it is essential to obtain and compare the annualized values of fuel costs, capital or carrying charges, and the operating and maintenance (O&M) expenditures. Within the system economic operating life, the component costs may vary significantly. Therefore, annualized values for all cost components should be used in the estimation and cost analysis optimization for proper economic analysis [50]. In this regard, the hourly capital investment (CI) cost for each component based on the actual annual number of operating hours (N) is calculated as:

$$\dot{Z}_k^{CI}(\$/h) = \frac{Z_k.CRF.\phi}{N} \quad (14)$$

The exergo-economic analysis is used to calculate the cost rate of the product streams of the system. The cost balance expresses the variable $\dot{C}$ that indicates a cost rate associated with an exergy stream: a stream of matter, power, or heat transfer. According to the conservative nature of costs [51], the cost rate associated with the system product $\dot{C}_P\left(\frac{\$}{h}\right)$ is equal to the total rate of expenditure used to generate this product in a component, namely the fuel cost resulting from the cost associated with the exergy flows $\dot{C}_F\left(\frac{\$}{h}\right)$ and the cost rates associated with the CI and OM as:

$$\dot{C}_P = \sum \dot{C}_F + \dot{Z}_k^{CI+OM} \quad (15)$$

The above cost balance equation is applied to the MED-MVC system components to obtain the product stream cost. Typically, the number of unknown cost parameters is higher than the number of cost balance equations for the component, so additional auxiliary thermodynamic equations are used to accommodate this difference. Usually, the auxiliary equations represent the equality of the average cost of the inlet and exit for the same stream, and they are formulated based on different principles (exergy extraction, multiple outputs, and external assessment) as shown in Table 4. To obtain the exergy definition equations for fuel and product for the MED-MVC components, all $\dot{C}$ in the fuel and product columns in Table 4 are replaced by $\dot{E}$ and linear system of equations are used to solve the exergy balance equation to obtain the component exergy destruction. For the mixing points, the product cost is considered as the summation of cost rate for the inlet points while for splitting points the outlet cost rate streams are equally divided. The exergy and cost balance equations for the inter-effects pumps in the cases of FF and PF are presented in Table 5.

To include the labor and chemical cost (non-exergy related costs) in the exergo-economic analysis, inlet feed stream to the feed pump is considered as $\dot{C}_o(\$/h) = (SLC + SCC)(\$/m^3) \times D(m^3/h)$. Also, the summation of the outlet stream flow rate cost must be equal to the sum of the carrying charges, fuel cost rate and the operating and maintenance calculated on a per hour basis to satisfy the cost rate balance for the total system [52]. Finally, the total water price ($\mathrm{TWP}_{exergo-economic}$) $(\$/m^3)$ from the exergo-economic analysis is calculated by dividing the cost rate of the product $(\$/h)$ from the distillate pump by the total production rate of the plant (m^3/h). The linear system of algebraic equations presented in Table 1 to Table 5 are solved by consideration of the cost of the electrical energy used for the pump and compressor as 0.08 $/kWh [53]. The results from the cost exergy model are sufficient for (a) providing more details from an economic standpoint to enable the calculation separately of the product stream cost at any intermediate state in the system; (b) understanding the cost formation process and the flow of costs in the system to highlight the involvement of each component in the final cost and offer an opportunity to identify the cost concentrated components that need attention to achieve a lower product cost [52]. Three important

parameters for evaluating the exergo-economic analysis of the thermal energy systems are calculated using the component exergetic efficiency (ϵ_k) and average cost per unit fuel exergy $c_{F,k}$. The variables include: the exergy destruction cost rate ($\dot{C}_{D,k}$), relative cost difference (r_k) and the exergo-economic factor (f_k) which are given by Eqs. (16)–(18) [52].

$$\dot{C}_{D,k} = c_{F,k}\dot{E}_{D,k} \tag{16}$$

$$r_k = \frac{1-\epsilon_k}{\epsilon_k} + \frac{\dot{Z}_k^{CI+OM}}{c_{F,k}\dot{E}_{P,k}} \tag{17}$$

$$f_k = \frac{\dot{Z}_k}{\dot{Z}_k + \dot{C}_{D,k}} \tag{18}$$

The r_k for a component represents the average cost per exergy unit between fuel and product and it is useful to evaluate and optimize a system component. The higher value of the total operating cost $\dot{C}_{D,k} + \dot{Z}_k$ indicates the higher influence of the component on the overall system performance, therefore in designing a new system, the first design changes must initially be applied to that component. The f_k is used to identify the relative significance of non-exergy related costs (CI&OM) to the sum of CI, O$M and the exergy destruction cost rate. A low value of f_k for major components suggests that the cost saving for the system could be accomplished by improving the components efficiency (reduction of exergy destruction) even if the capital cost investment increases [52].

Table 4 Fuel and product cost rates of the MED-MVC system components.

		Fuel	Product	Capital and investment	Auxiliary equation
Feed pump		$C_e.\dot{W}_{FP} + \dot{C}_o$	$\dot{C}_1$	$\dot{Z}_{FP}$	--
Brine pump		$C_e.\dot{W}_{BP} + \dot{C}_{11}$	$\dot{C}_{12}$	$\dot{Z}_{BP}$	--
Distillate pump		$C_e.\dot{W}_{DP} + \dot{C}_8$	$\dot{C}_9$	$\dot{Z}_{DP}$	--
MVC unit		$C_e.\dot{W}_{compressor} + \dot{C}_{13}$	$\dot{C}_{14}$	$\dot{Z}_{compressor}$	--
Brine heater		$\dot{C}_3 + \dot{C}_{10}$	$\dot{C}_5 + \dot{C}_{11}$	$\dot{Z}_{F/B}$	$\frac{\dot{C}_{10}}{\dot{E}_{10}} = \frac{\dot{C}_{11}}{\dot{E}_{11}}$
distillate heater		$\dot{C}_2 + \dot{C}_7$	$\dot{C}_4 + \dot{C}_8$	$\dot{Z}_{F/D}$	$\frac{\dot{C}_7}{\dot{E}_7} = \frac{\dot{C}_8}{\dot{E}_8}$
1st effect	BF	$\dot{C}_{19} + \dot{C}_{14}$	$\dot{C}_{15} + \dot{C}_{16} + \dot{C}_{10}$	$\dot{Z}_{Ev,1}$	$\frac{\dot{C}_{14}}{\dot{E}_{14}} = \frac{\dot{C}_{15}}{\dot{E}_{15}}$ & $\frac{\dot{C}_{19}}{\dot{E}_{19}} = \frac{\dot{C}_{10}}{\dot{E}_{10}}$
	FF	$\dot{C}_6 + \dot{C}_{14}$	$\dot{C}_{15} + \dot{C}_{16} + \dot{C}_{18}$		$\frac{\dot{C}_{14}}{\dot{E}_{14}} = \frac{\dot{C}_{15}}{\dot{E}_{15}}$ & $\frac{\dot{C}_6}{\dot{E}_6} = \frac{\dot{C}_{18}}{\dot{E}_{18}}$
	PF / PCF	$\dot{C}_{6'} + \dot{C}_{14}$			$\frac{\dot{C}_{14}}{\dot{E}_{14}} = \frac{\dot{C}_{15}}{\dot{E}_{15}}$ & $\frac{\dot{C}_{6'}}{\dot{E}_{6'}} = \frac{\dot{C}_{18}}{\dot{E}_{18}}$
2nd effect	BF	$\dot{C}_{16} + \dot{C}_{23}$	$\dot{C}_{17} + \dot{C}_{18} + \dot{C}_{20}$	$\dot{Z}_{Ev,2}$	$\frac{\dot{C}_{16}}{\dot{E}_{16}} = \frac{\dot{C}_{17}}{\dot{E}_{17}}$ & $\frac{\dot{C}_{23}}{\dot{E}_{23}} = \frac{\dot{C}_{18}}{\dot{E}_{18}}$

	FF	$\dot{C}_{16}+\dot{C}_{19}$	$\dot{C}_{17}+\dot{C}_{20}+\dot{C}_{22}$		$\frac{\dot{C}_{16}}{\dot{E}_{16}}=\frac{\dot{C}_{17}}{\dot{E}_{17}}$ & $\frac{\dot{C}_{19}}{\dot{E}_{19}}=\frac{\dot{C}_{22}}{\dot{E}_{22}}$
	PF	$\dot{C}_{\acute{6}}+\dot{C}_{16}$	$\dot{C}_{17}+\dot{C}_{19}+\dot{C}_{21}$		$\frac{\dot{C}_{16}}{\dot{E}_{16}}=\frac{\dot{C}_{17}}{\dot{E}_{17}}$ & $\frac{\dot{C}_{\acute{6}}}{\dot{E}_{\acute{6}}}=\frac{\dot{C}_{21}}{\dot{E}_{21}}$
	PCF	$\dot{C}_{\acute{6}}+\dot{C}_{16}+\dot{C}_{18}$			
3rd effect	BF	$\dot{C}_{20}+\dot{C}_{27}$	$\dot{C}_{21}+\dot{C}_{24}+\dot{C}_{22}$	$\dot{Z}_{Ev,3}$	$\frac{\dot{C}_{20}}{\dot{E}_{20}}=\frac{\dot{C}_{21}}{\dot{E}_{21}}$ & $\frac{\dot{C}_{22}}{\dot{E}_{22}}=\frac{\dot{C}_{27}}{\dot{E}_{27}}$
	FF	$\dot{C}_{20}+\dot{C}_{23}$	$\dot{C}_{21}+\dot{C}_{24}+\dot{C}_{26}$		$\frac{\dot{C}_{20}}{\dot{E}_{20}}=\frac{\dot{C}_{21}}{\dot{E}_{21}}$ & $\frac{\dot{C}_{23}}{\dot{E}_{23}}=\frac{\dot{C}_{26}}{\dot{E}_{26}}$
	PF	$\dot{C}_{\acute{6}}+\dot{C}_{19}$	$\dot{C}_{20}+\dot{C}_{22}+\dot{C}_{24}$		$\frac{\dot{C}_{19}}{\dot{E}_{19}}=\frac{\dot{C}_{20}}{\dot{E}_{20}}$ & $\frac{\dot{C}_{\acute{6}}}{\dot{E}_{\acute{6}}}=\frac{\dot{C}_{24}}{\dot{E}_{24}}$
	PCF	$\dot{C}_{\acute{6}}+\dot{C}_{19}+\dot{C}_{21}$			
4th effect	BF	$\dot{C}_{6}+\dot{C}_{24}$	$\dot{C}_{13}+\dot{C}_{25}+\dot{C}_{26}$	$\dot{Z}_{Ev,4}$	$\frac{\dot{C}_{24}}{\dot{E}_{24}}=\frac{\dot{C}_{25}}{\dot{E}_{25}}$ & $\frac{\dot{C}_{6}}{\dot{E}_{6}}=\frac{\dot{C}_{26}}{\dot{E}_{26}}$
	FF	$\dot{C}_{24}+\dot{C}_{27}$	$\dot{C}_{13}+\dot{C}_{10}+\dot{C}_{25}$		$\frac{\dot{C}_{24}}{\dot{E}_{24}}=\frac{\dot{C}_{25}}{\dot{E}_{25}}$ & $\frac{\dot{C}_{27}}{\dot{E}_{27}}=\frac{\dot{C}_{10}}{\dot{E}_{10}}$
	PF	$\dot{C}_{\acute{6}}+\dot{C}_{22}$	$\dot{C}_{23}+\dot{C}_{13}+\dot{C}_{25}$		$\frac{\dot{C}_{22}}{\dot{E}_{22}}=\frac{\dot{C}_{23}}{\dot{E}_{23}}$ & $\frac{\dot{C}_{\acute{6}}}{\dot{E}_{\acute{6}}}=\frac{\dot{C}_{25}}{\dot{E}_{25}}$
	PCF	$\dot{C}_{\acute{6}}+\dot{C}_{22}+\dot{C}_{24}$	$\dot{C}_{23}+\dot{C}_{13}+\dot{C}_{10}$		$\frac{\dot{C}_{22}}{\dot{E}_{22}}=\frac{\dot{C}_{23}}{\dot{E}_{23}}$ & $\frac{\dot{C}_{\acute{6}}}{\dot{E}_{\acute{6}}}=\frac{\dot{C}_{10}}{\dot{E}_{10}}$

Table 5 Cost and exergy balance equations for inter-effects pumps for BF and FF MED-MVC systems

Configuration	Exergy balance	Cost rate balance
Pump1	$\dot{E}_{D,P1}=\dot{E}_{18}+\dot{W}_{P1}-\dot{E}_{19}$	$\dot{C}_{19}=\dot{C}_{18}+C_e.\dot{W}_{P1}+\dot{Z}_{P1}$
Pump2	$\dot{E}_{D,P2}=\dot{E}_{22}+\dot{W}_{P2}-\dot{E}_{23}$	$\dot{C}_{23}=\dot{C}_{22}+C_e.\dot{W}_{P2}+\dot{Z}_{P2}$
Pump3	$\dot{E}_{D,P3}=\dot{E}_{26}+\dot{W}_{P3}-\dot{E}_{27}$	$\dot{C}_{27}=\dot{C}_{26}+C_e.\dot{W}_{P3}+\dot{Z}_{P3}$

iii. Aggregation level exergy cost model

Exergy cost model can be applied considering only the overall system as a group of components (MED-MVC plant as a whole unit) [52]. To study the effect of the aggregation level on the cost estimation, consider an overall system as shown in Fig. 4 for the MED-MVC system. The cost rate balance for the MED-MVC system using the aggregation level is as follows:

$$\dot{C}_9=\dot{C}_0+\dot{Z}_{total}^{CI+O\&M}+C_e.\left(\dot{W}_{\text{compressor}}+\dot{W}_{pumps}\right)-\dot{C}_{12} \quad (19)$$

where $\dot{Z}_{total}^{CI+O\&M}$ represents the hourly CI cost and OM for all MED-MVC components.

The previous equation involves two unknowns: the cost per exergy unit associated with brine and distillate streams. Therefore, one auxiliary relation is required before these unknowns can be determined. For simplicity the auxiliary equation for this aggregated system is considered as: $\frac{\dot{C}_{12}}{\dot{E}_{12}}=\frac{\dot{C}_9}{\dot{E}_9}$.

The total water price from aggregation method ($TWP_{aggregation}$) ($\$/m^3$) is calculated by dividing the cost rate of all the outlet streams (distillate and brine) ($\$/h$) by the total production rate (D) of the plant (m^3/h). Equation (19) could represent any desalination system that uses electricity to produce fresh water.

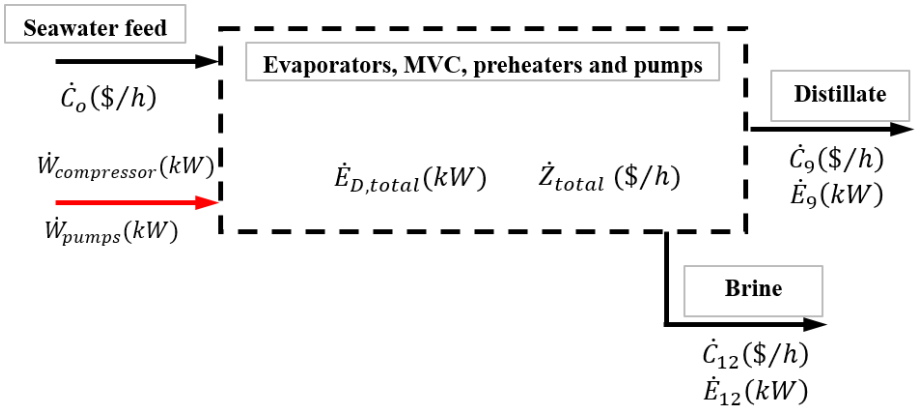

Fig. 4 Aggregation level for exergy costing for MED-MVC system

4. Results and discussion

4.1 Model validation

As a first step to validate the developed model using the Engineering Equation Solver (EES) software, a comparison is made between the calculated and actual parameters of two MVC systems available in the literature. As shown in Table 6, the single-effect MVC model provides predictions very close to the actual data reported for a MVC plant located in Spain [8]. Furthermore, the results from the MED-MVC model compare very well with the actual operational parameters of a two-effect MED-MVC plant located in India operating in the PCF configuration [54]. The current models are therefore validated because the maximum deviation between the model predictions and the actual data is under 7%.

Table 6 Validation of the single-effect MVC and MED-MVC with PCF configuration models.

Parameter	**1-effect MVC**	**Veza [8]**	**% error**	**2-effect MVC**	**Kishore et al. [54]**	**% error**
Inlet feed salinity, g/kg	38		-	35		-
Outlet brine salinity, g/kg	65		-	70		-
Steam temperature T_s, °C	61.1		-	65.0		-
last brine temperature T_n, °C	-		-	60.0		-
Pressure ratio	1.1			1.26		
Distillate production, (D)m^3/h	20.92	20.8	0.6	2.03	2.09	2.9
Feed flow (F), m^3/h	50.37	50	0.75	4.06	4.16	2.4
Brine flow (B), m^3/h	29.45	29	1.6	2.03	2.08	2.4
Feed temperature T_f, °C	53.7	55	2.4	56.0	NA	-
Compressor work ($\dot{W}_{comp}$), kW	228	240	5	29.59	28.41	4.2

Performance ratio PR	0.89	NA	-	1.83	NA	-
heat transfer area, $m^2/kg/s$	469.9	448.9	4.7	371.1	349.8	6.1
Total SPC, kWh/m^3	13.25	14	5.4	14.57	13.64	6.8
Total water price (TWP), $\$/m^3$	2.69	2.8	3.9	2.34	NA	-

4.2 Energetic and exergetic analysis

The current work is focused on modeling of MED-MVC systems operating with four different feed configurations using the first and second law of thermodynamics accompanied with exergo-economic analysis. The developed model is applied to a MED-MVC system with four effects. The different feed arrangements are compared to identify the most reliable configuration considering energetic and exergo-economic analysis for cost flow rate for each component. The steady-state input operating conditions (base case) adopted for all configurations are shown in Table 7. These conditions are obtained from an actual MED-MVC plant located in France [9]. From the 1st law energy analysis, the PCF and FF configurations require less work to produce the same amount of distillate. The PR also compares favorably to the other configurations as shown in Table 7. The calculated SPC values are 30.1, 13.7, 23 and 13.9 kWh/m^3 for the BF, FF, PF and PCF configuration, respectively. The required compressor work for the BF configuration is the highest which is due to the increase in the E_{SH} term to compensate for the small value of vapor flow rate recovered from the last effect. On the other hand, the FF requires the lowest work to achieve the same production capacity. Changing the feed arrangement from BF to FF and PF to PCF at a constant compression ratio, the SPC is reduced by 54% and 39%, respectively. The FF configuration has the highest electric power needed to operate the feed, brine, distillate pumps as well as the inter-effects pumps. The performances of the MED-MVC operating in the PCF and FF configurations are comparable and are higher than those in the BF and PF configurations. This is primarily due to the decrease in compressor work consumption and the more efficient reuse of the hot brine. In the FF and PCF configurations, the hot brine passes in the forward direction where the pressure decreases from one effect to the next which allows brine flashing to occur.

Table 7 Steady-state specifications of MED-MVC different process configurations.

Configuration	BF	FF	PF	PCF
Number of effects (N)		4		
Inlet feed content, g/kg		36		
Outlet brine content, g/kg		65		
Inlet steam temperature T_s, °C		62.5		
last brine temperature T_n, °C		50.3		
Feed temperature T_f, °C		49		
Pressure ratio		1.852		
Distillate production, (D)m^3/h		63.36		
Feed flow (F), m^3/h		141.98		
Brine flow (B), m^3/h		78.66		
Heat source flow rate (S), kg/s	4.12	4.6	4.27	4.35
Performance ratio PR	2.89	3.19	3.02	3.33
Specific heat transfer area (S_A), $m^2/kg/s$	288.9	260.2	211	227.2
Compressor actual work (W_a), kW	1873	845.1	1430	862
Pumps work, kW	10.4	13.1	7.5	7.5

The first step in any improvement or enhancement project is diagnostics, and the most powerful diagnostics tool in thermodynamics is second law analysis. Exergy analysis overcomes many of the shortcomings of energy analysis and identifies the causes, locations and actual magnitudes of waste due to thermodynamic inefficiency [55]. Starting with the minimum work of separation $\dot{W}_{min}$ for the separation of 39.4 kg/s of seawater into 17.6 kg/s of fresh water and 21.8 kg/s of brine with a salinity of 65 ppt at the same temperature and pressure. The value of $\dot{W}_{min}$was determined independently using the relation developed by Cerci [56] as 28.2 kW for recovery ratio of ~40%. For the BF, FF, PF and PCF configurations, the value of $\dot{W}_{min}$ obtained from equation (13) is 44.8, 22.4, 34.6 and 23.7 kW, respectively. The exergy analysis was carried out to estimate the component irreversibilities to obtain the rates of exergy destruction and the percentage of each component so that the locations with the highest exergy destruction can easily be identified for the MED-MVC system with different feed configurations as shown in Fig. 5.

Generally, there are two causes of exergy destruction in the MED-MVC systems. The first is heat transfer across the temperature difference between hot and cold streams in each evaporator effect and the preheaters, resulting in process irreversibility. In addition, exergy destructions in the pumps and compressor are due to irreversibilities in the compression process. The second is the exergy discharge, through brine and distillate, into the environment. The MVC unit and evaporators are significant sources of exergy destruction in the MED-MVC systems which range between 86 and 90% for all configurations. These high levels can be

attributed to the thermodynamic inefficiency of the MVC unit and the heat transfer in the effects that are associated with phase change process. MVC has the highest exergy destruction percentages for the BF and PF configurations while the percentages are lower at the evaporators. The reverse is true for the FF and PCF configurations. For all configurations, the first effect has the highest exergy destruction among the four effects. The high exergy destructions in the evaporators indicate that the evaporation process itself is highly inefficient. Therefore, modifications and improvements to the process should be considered. The exergy destruction can be reduced by increasing the number of effects, though the number is limited by the compression ratio of MVC units currently available. Also, if the temperature difference within each effect is lowered to reduce exergy destruction, economic consideration due to increasing the heat transfer surface needed to achieve evaporation and condensation processes should be accounted. Other components such as brine and distillate feed heaters have the second lowest share in the exergy destruction of the systems that range between 7.6 and 10.9% for all configurations. The exergy destruction for both feed heaters changes slightly with feed configuration due to the constant flow rates and the small differences in the hot and cold side flow stream temperatures. Moreover, Fig. 5 shows that the exergy destruction in the pumps accounts for a negligible share of the total exergy destruction for the PCF and PF configurations. However, due to inter-effects pumps in BF and FF configurations, exergy destruction percentage due to pumps increases to 1.63 and 3.76%, respectively, compared to the PF and PCF configurations without inter-effects pumps.

By calculating the second law efficiency for all configurations, the results show that the PCF configuration has the highest value followed by the FF configuration, while the BF configuration exhibits the lowest value among all configurations. This indicates how crossing the hot brine between effects to acquire its energy through flashing is beneficial in both increasing the evaporation amount in each effect and in improving the total system performance. Furthermore, it should be noted that the calculated exergetic efficiency is quite low as 2.38, 2.73, 2.4 and 2.92% for the BF, FF, PF and PCF configurations, respectively. These values are close to the exergetic efficiency presented in Refs. [22, 57, 58] for similar plants. The performance and

economics of the MED–MVC system are compared to those of conventional MED and MED-TVC systems with a similar capacity. The considered MED and MED-TVC systems operated in the PCF configuration with a bottom condenser and were investigated using a model developed by El-Dessouky and Ettouney [39] under the similar constraints for the same freshwater production (17.6 kg/s) and rejected brine salinity (65 ppt). The simulation shows that the required mass flow rate of the steam supplied to the 1st effect is 5.13 and 2.7 kg/s for MED and MED-TVC, respectively compared to 4.4 kg/s in case of MED-MVC. To account for the difference in input energy of MED (steam) and MED-MVC (electrical), the input exergy definition for MED-MVC is modified by assuming the thermal efficiency for the power plant supplying the electrical energy to the MVC unit is equal to 40%. The calculated values of gained output ratio (GOR=fresh water per steam required) and TWP for fresh water generation of 1500 m^3/d are 3.99[-] and 1.6 \$/m^3 for MED–MVC, 3.43[-] and 3.1 \$/m^3 for conventional MED and 6.4[-] and 2.6 \$/m^3 for MED-TVC as reported in [59, 60]. The MED-MVC saves approximately 50% in the cost of freshwater production compared to the conventional MED system. Furthermore, no condenser is required for heat rejection as in the conventional MED or MED-TVC systems. However, from the exergy point of view, the exergy efficiency of MED–MVC (2.9%) is much lower than the conventional MED (11.9%) or MED-TVC (4.6%). The low exergy efficiency is due to the fact that the MED-MVC systems are inefficient as they convert electrical energy into thermal energy.

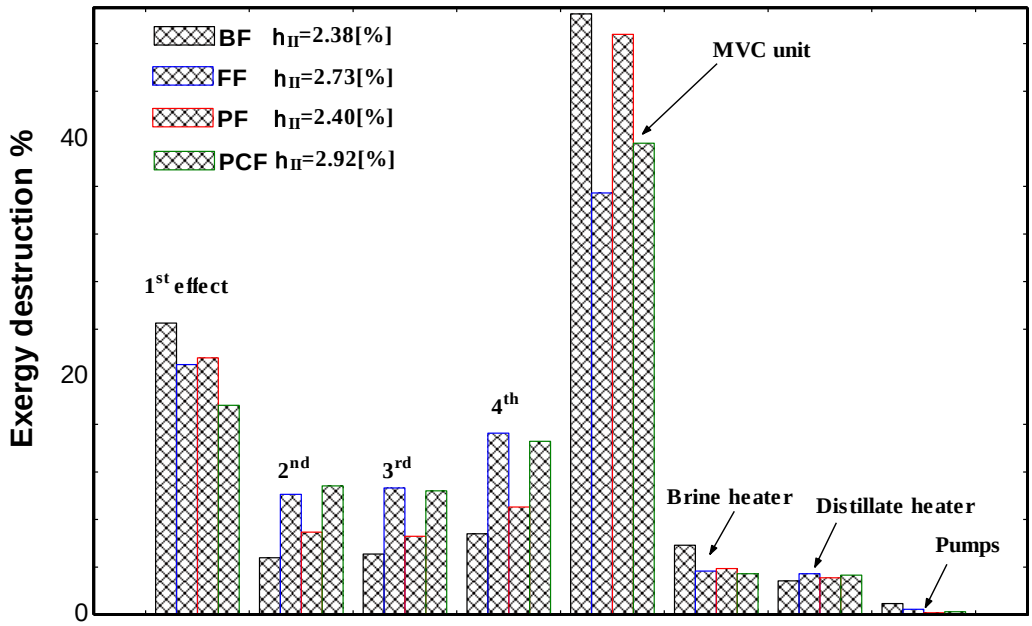

Fig. 5 Percentage of exergy destruction for main component of various feed MED-MVC systems.

4.3 Economic and exergo-economic analysis

The component costs on the hourly basis for different feed configurations are presented in Table 8. The most expensive components are the evaporators and compressor, and the cheapest equipment is the pumps. For the BF and PF arrangements, the price of the MVC unit is high due to the high actual work required to achieve the given fresh water production. The fixed cost for the BF is the highest compared to other configurations. Also, Table 8 illustrates that by changing the feed arrangement from BF to FF and PF to PCF at a constant compression ratio, the total fixed cost for the MED-MVC plant is reduced by ~ 30% and 17%, respectively.

Table 8 Fixed cost rate per hour basis for different feed configurations MED-MVC system components.

Component	BF	FF	PF	PCF
Feed pump		0.17		
Brine pump		0.13		
Distillate pump		0.11		
MVC unit	20.9	9.7	15.9	10.0
Brine heater	0.5	0.75	0.6	0.75
Distillate heater	0.54	1.0	0.67	1.0
1st effect	7.63	4.13	3.7	3.6
2nd effect	4.8	4.31	3.1	3.0
3rd effect	3.8	4.48	3.5	3.5
4th effect	3.5	4.67	3.8	3.8

Inter-effects pumps	0.25	0.27	--	--
Total ($/h)	42.4	29.7	31.7	26.2

A simple conventional economic model treating the MED-MVC plant as a whole unit is used to calculate the annualized cost of the plant and to estimate the total water price for a MED-MVC system. The model shows that changing the plant layout by moving from BF to FF or from PF to PCF will reduce the TWP estimated from the economic model by 45% or 31%, respectively as shown in Table 9. However, to indicate the share of each flow stream and each component in the total cost of the product, the economic analysis based on exergy is applied to all MED-MVC configurations. When conducting a thermoeconomic analysis for the current MED-MVC system, a cost balance equation is used to correlate the exergy instead of the energy of the flow stream with the pricing value of a component. This cost balance, combined with appropriate auxiliary thermo-economic relations, result in a system of linear algebraic equations, which can be solved for the unknown values of cost rates or of cost per exergy unit. As mentioned before, non-exergy related costs including chemical cost and labor cost are added to the exergo-economic model as input stream in the feed seawater. Further, it should be mentioned that there is no additional information to appropriately apportion the value of other cost and indirect cost between the product streams (distillate and brine) in the cost exergy equations. The other cost (80k $) and indirect cost (0.15DCC) are calculated on a per hour basis, and a value of 3.59 $/h is obtained. For simplicity, these costs are divided equally between the distillate and brine streams to adjust the final distillate stream price. Solving the exergy-cost balance equations, the cost rates for the various stream at different locations in the MED-MVC plant are obtained.

The effects of variation of the economic parameters such as cost index factor (C_{index}), interest rate (i), and electricity cost (C_e) on the TWP for different feed configurations of a MED-MVC system are presented in Fig. 6. The cost index and interest rate affect the fixed cost and the capital investment of the plant while electricity cost affects the plant operating cost. Increasing the cost index from 1 to 2 has a smaller effect than a change in interest rate. Increasing the interest rate from 2 to 15% translates to a total water price increase in the range of 22 to 28%. The fuel cost to operate a MED-MVC plant (electricity cost) depends

on the plant location associated with different electricity production prices. The main energy consumption of a MED-MVC desalination system is represented by the electricity requirement which is required to operate the MVC unit and the installed pumps. Increasing the electricity cost has a significant effect on the TWP compared to other economic parameters. For low values of C_e, the PF and FF configurations have a TWP of ~1 \$/m^3 and PCF has a TWP of 0.77 \$/m^3. On the other hand, for high values of C_e, the FF and PCF configurations have nearly the same TWP. This could be explained as follows, for low price of electricity, the cost of evaporator installation (heat transfer area) dominates the water production price; while for high price of electricity, the cost of the MVC unit dominates the TWP for the same plant capacity. If the MED-MVC with the PCF configuration is integrated to a power generation cycle in two regions with a different price of $C_e = 0.03$ and 0.09 \$/kWh, the TWP will be 0.92 and 1.85 \$/m^3, respectively. A 200% increase in C_e increases the TWP by approximately 100%. These results reveal that the most important parameter that cannot be neglected while comparing different installation areas for MVC systems is the electricity cost.

Using average values of the economic parameters (C_{index} =1.2, i=5% and C_e=0.08 \$/kWh), the cost rate pricing for the FF, PF and PCF configurations for all flow streams through the MED-MVC system are shown in Fig. 7. Also, Table 9 shows the final estimated total water price using the three methods (simple conventional economic model, exergy-based component cost model and exergy aggregation model). These estimates are consistent with the results for thermal desalination units found in the literature [22, 46, 61]. Besides showing the cost flow rate at each stream point, Fig. 7 shows the flow exergy, temperature and stream flow rate as well. To some extent, the three economic models yield similar estimates for the TWP. However, it is preferable to apply exergy costing on the component level rather than only components grouping. Also, the aggregation formulation does not consider the essential information related to how the actual processes occur and the actual cost formation process in the system. Furthermore, the differences

between exergy-based component cost and simple cost model are directly attributed to the assumptions used such as auxiliary equations and the uncertainty associated with the cost due to round-off [52].

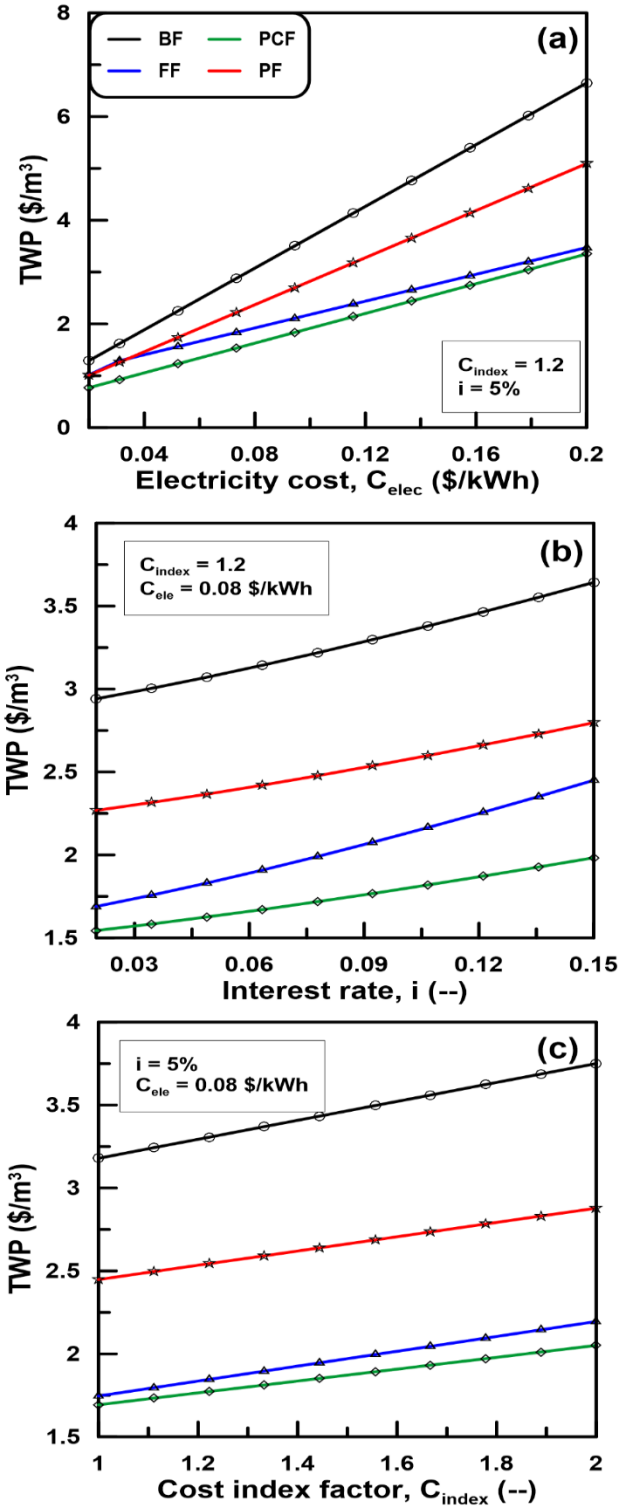

Fig. 6 Effect of economic parameters on TWP for different feed configurations of MED-MVC system.

Table 9 Total water price for different MED-MVC process configurations and different cost models.

Configuration	**BF**	**FF**	**PF**	**PCF**
TWP using simple method, $/m^3	3.19	1.73	2.46	1.7
$TWP_{exergo-economic}$, $/m^3	3.08	1.81	2.53	1.77
$TWP_{aggregation}$, $/m^3	2.85	1.53	2.15	1.62

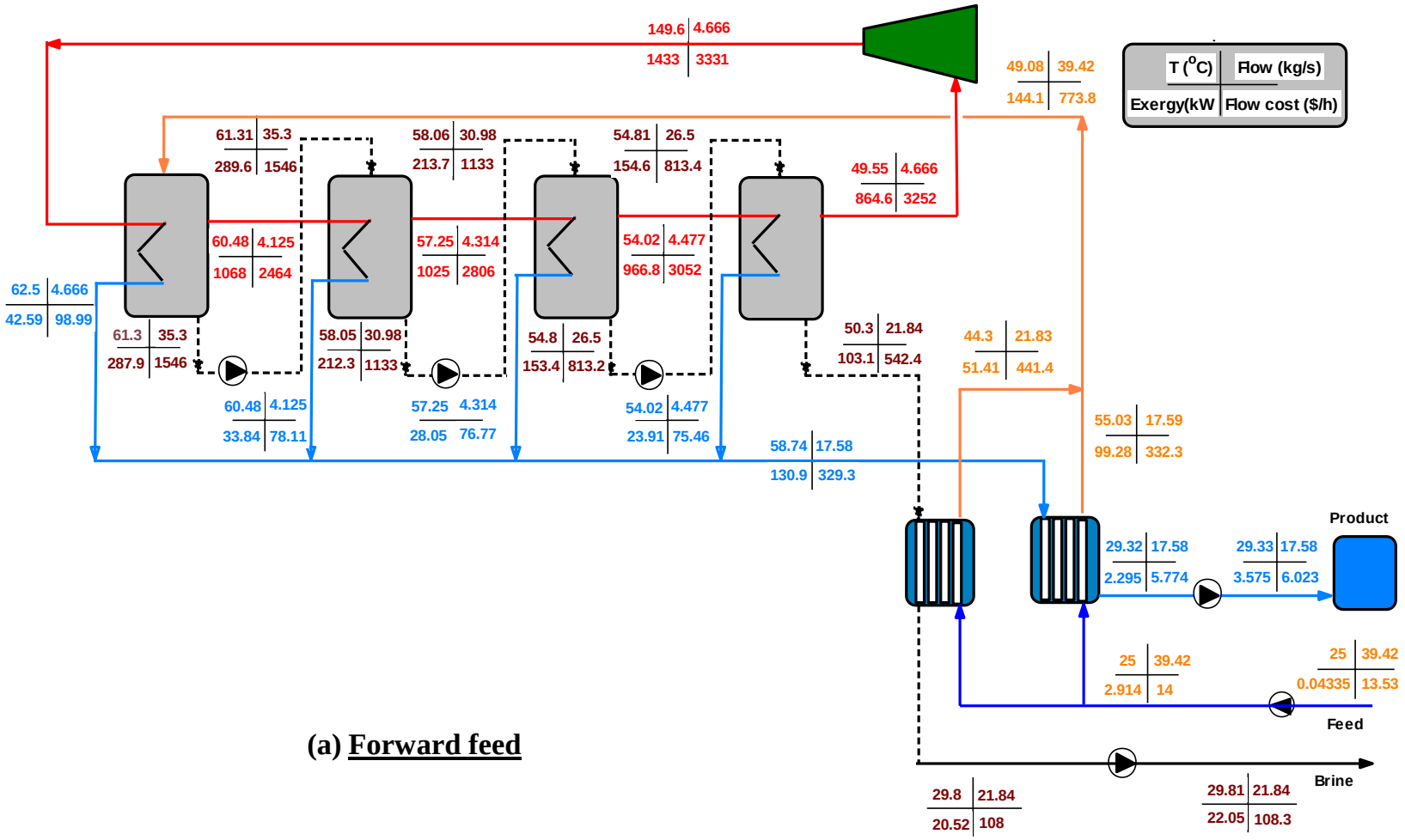

Fig. 7 Cost flow diagram for MED-MVC system with (a) FF, (b) PF and (c) PCF configurations.

Fig. 7 continued

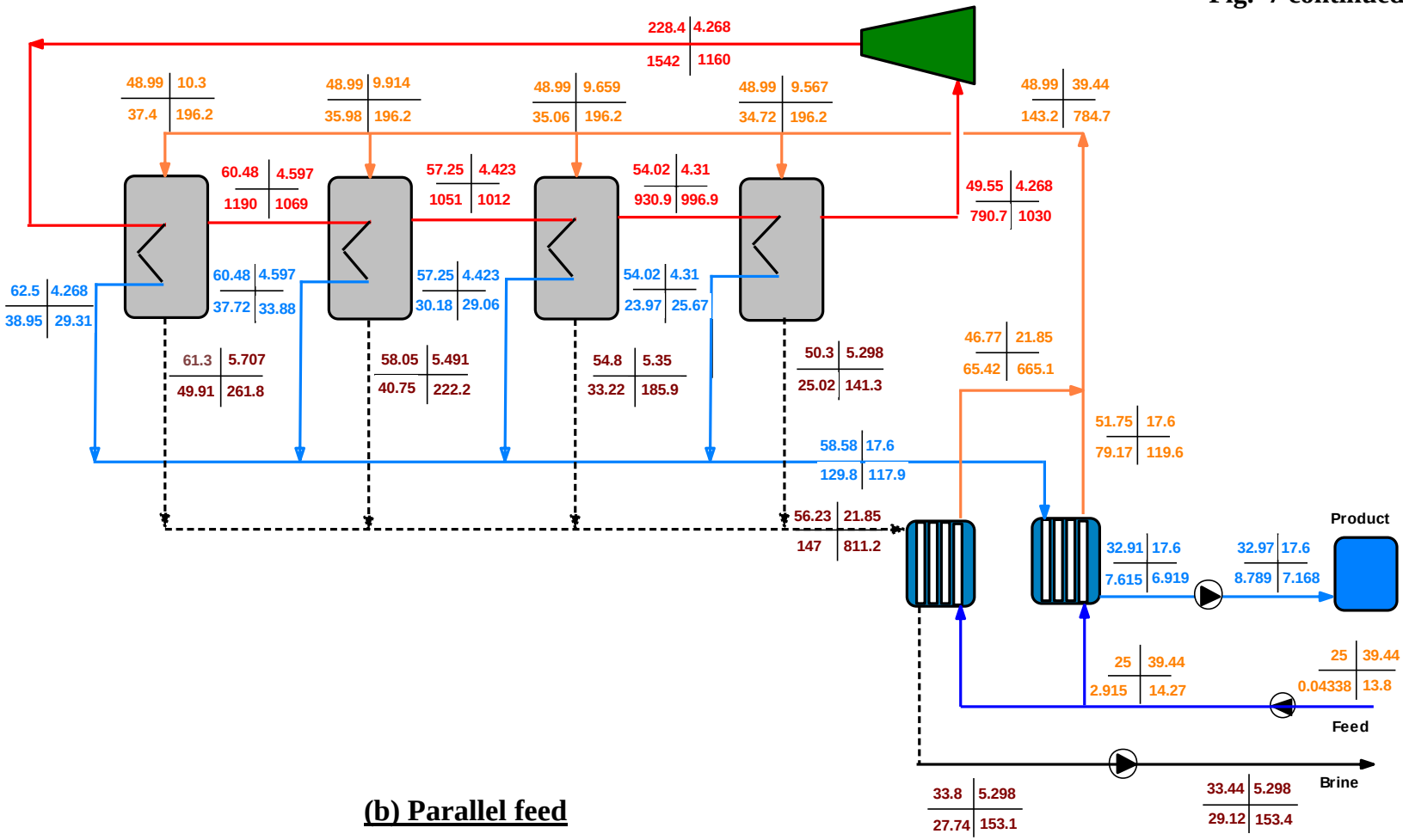

(b) Parallel feed

Fig. 7 continued

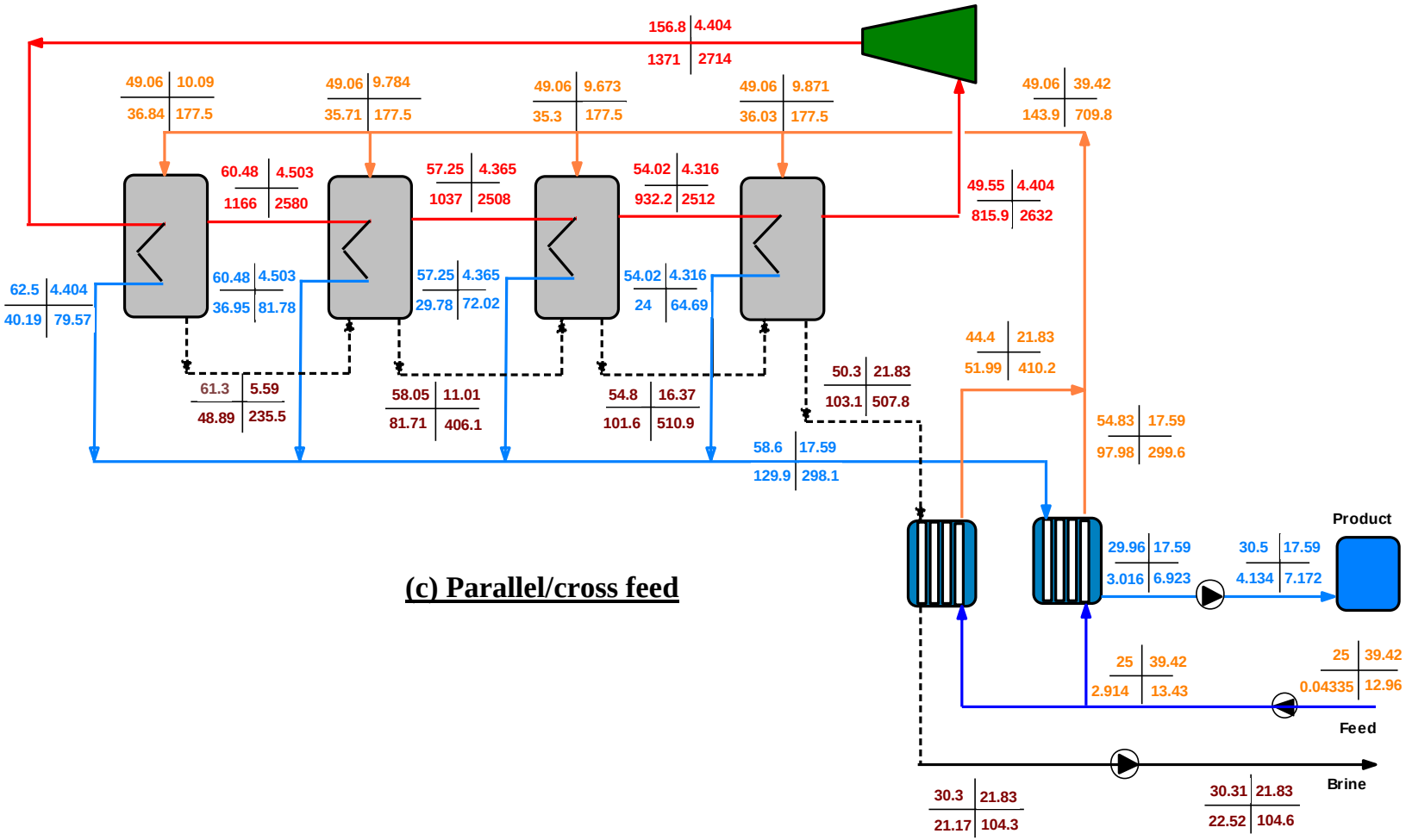

(c) Parallel/cross feed

The exergo-economic parameters of the MED-MVC system operating in PCF and FF configurations are calculated for the base case as shown in Table 10. The calculated parameters for each component include the component second law efficiency ϵ_k, exergy destruction $\dot{E}_{D,k}$, cost per unit fuel exergy $c_{F,k}$, cost per unit product exergy $c_{P,k}$, exergy destruction cost rate $\dot{C}_{D,k}$, investment and O&M cost rate $\dot{Z}_k$, relative cost difference factor r_k, and exergo-economic factor f_k. For the PCF configuration, the last effect has highest values of the sum $\dot{Z}_k + \dot{C}_{D,k}$ among the evaporators while for the FF configuration it is the first effect. For both configurations, MVC unit has the highest values of $\dot{Z}_k + \dot{C}_{D,k}$ which is considered the most important component from the thermo-economic point of view in the MED-MVC systems. The lower values of the variable f_k for the MVC unit, brine preheater and distillate preheater show that the cost associated with these components is dominated by the exergy destruction. The remaining part is caused by $\dot{Z}_k$value of the component as indicated for both feed configurations. So, it can be concluded that, reducing the exergy destruction in these components could be cost effective for the complete system even if this would increase the investment costs associated with these components. For the evaporator units, the high values of $\dot{Z}_k + \dot{C}_{D,k}$ and the relatively small values of factor f_k suggest that the exergy destruction cost dominates the investment and O&M cost. According to the cost model assumption, the capital investment costs for the evaporators depend on the evaporator areas and the overall heat transfer coefficients. Therefore, modifications and improvements to the heat transfer process should be considered. For the FF configuration, the inter-effect pumps have highexergetic efficiency but also it has the lowest f_k, which indicate that the exergy destruction costs are controlling even with a relatively high exergetic efficiency of the component. One important conclusion which can be drawn from the results presented in Table 10 is that thermo-economic analysis aims at identifying the possible reduction of sub-components total costs. This reduction can be either for the components inefficiency cost or the cost of components operating, whichever is controlling. Therefore, for components such as pumps, improvement is achieved by reducing the owning and operating cost of the sub-system under consideration at a cost of

reduction in the thermodynamic efficiencies. For components such as MVC, brine/distillate preheaters where component inefficiency is the dominant cost, improvement to reduce inefficiency costs can be obtained by improving the thermodynamic efficiency or the operating condition. Finally, it is noted that the values obtained for f_k and r_k parameters are close the values reported in [58].

Table 10 Exergo-economic variables for MED-MVC systems with FF and PCF feed configurations.

	Component	$\dot{E}_{D,k}(kW)$	$\epsilon_k(\%)$	$c_{F,k}(\$\ MJ^{-1})$	$c_{P,k}(\$\ MJ^{-1})$	$\dot{C}_{D,k} + \dot{Z}_k(\$/h)$	$r_k(\%)$	$f_k(\%)$
FF	MVC unit	301.9	65.3	0.42	0.5	460.9	21.5	2.1
	Distillate heater	29.3	77.2	1.03	1.05	114.7	30.5	0.89
	Brine heater	31.2	62.2	1.2	1.9	145.0	45.9	0.52
	1st effect	179	87.1	0.50	0.55	328.2	13.0	1.26
	2nd effect	86.1	91.7	0.55	0.57	157.7	6.2	2.74
	3rd effect	90.6	91	0.57	0.67	176.6	7.5	2.54
	4th effect	130	86.2	0.67	0.81	304.5	12.7	1.53
	Feed pump	0.87	76.7	0.64	1.2	1.6	21.6	11.0
	Distillate pump	0.44	74.6	0.28	0.54	1.7	58.6	6.42
	Brine pump	0.51	75.1	0.74	1.4	4.8	8.8	2.6
	P1	0.75	69.2	0.68	1.37	23.9	3.5	0.41
	P2	0.65	69.6	0.7	1.41	19.7	3.8	0.46
	P3	0.59	67.8	0.72	1.45	15.8	4.12	0.53
PCF	MVC unit	345	61.7	0.46	0.55	580.3	25.6	1.73
	Distillate heater	28.9	77.2	1.06	1.1	117.2	30.2	0.86
	Brine heater	30.0	63.4	1.17	1.78	134.0	43.5	0.56
	1st effect	153.1	88.5	0.55	0.61	306.7	12.3	1.18
	2nd effect	94.25	91.7	0.61	0.6	211.7	8.2	1.5
	3rd effect	90.64	91.0	0.67	0.75	222.7	8.6	1.5
	4th effect	126.8	86.0	0.75	0.89	345.5	13.6	1.1
	Feed pump	0.87	76.7	0.64	1.2	1.8	24.8	9.9
	Distillate pump	0.6	65.1	0.33	0.53	1.3	30.2	8.4
	Brine pump	0.68	66.4	0.7	1.3	3.4	6.2	3.7

4.4 Sensitivity analysis

The primary goal in the analysis of the MED-MVC desalination system is to reduce the operation and capital costs. The operation cost can be reduced by increasing the performance ratio or decreasing the SPC. The primary contributor to the SPC in a MED-MVC system is the power consumed by the MVC unit which depends on the compressor efficiency, compression ratio and inlet vapor specific volume.

Therefore, efforts are made to reduce the cost associated with the MVC. This can be done by reducing the vapor flow rate through the MVC unit by installing more effects N while keeping a constant overall temperature difference. On the other hand, capital cost can be reduced by reducing the required specific heat transfer area for evaporators and pre-heaters units. For MED-MVC, to decrease the S_A, the TBT must be increased. The increase in TBT will increase specific chemical pre-treatment costs and may add cost over the tube material and maintenance. Increasing N has its limits as this increases the required S_A for evaporation due to the decrease in the temperature difference between effects. Consequently, the capital costs savings would be overcome by the operating cost increase. It is essential to determine the optimal balance design parameters of N and TBT that achieve the optimum economic operation. The decrease in the SPC with increasing the number of effects N has its limit as shown in Fig. 8 for both FF and PCF configurations.

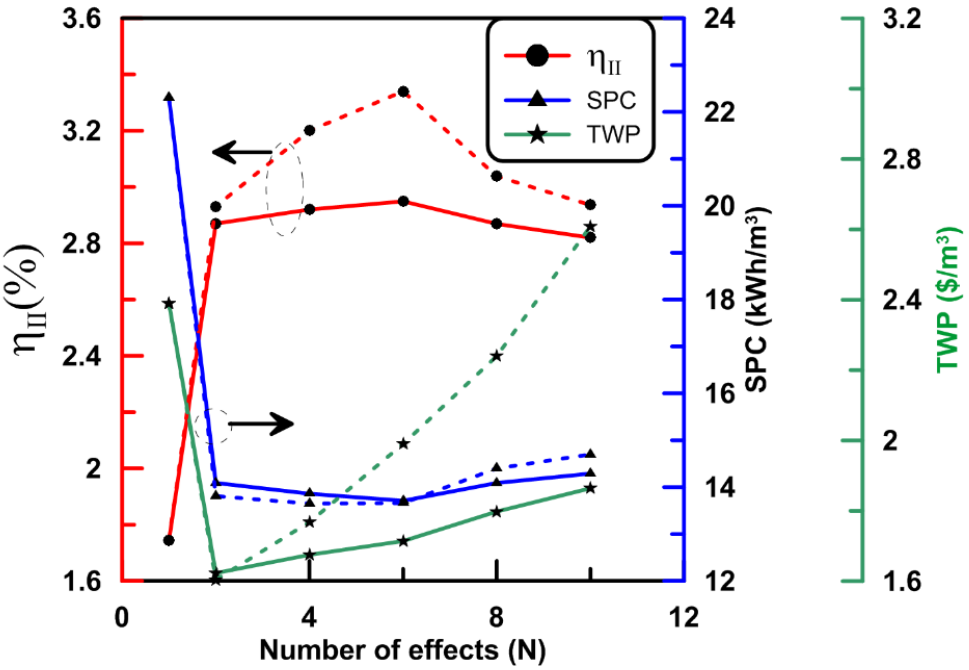

Fig. 8 Effect of number of effects on SPC, η_{II} and, TWP(Dash line FF, Solid line PCF).

A single-effect MVC has the maximum SPC due to the amount of vapor flow (displacement volume) through the MVC unit, leading to a high TWP of 2.4 $/m^3. Adding another effect for the same overall temperature difference increases the second law efficiency for both feed configurations by around 61% and reduces the SPC by 39%. Although this increases the specific heat transfer area by 67%, the TWP

reduces to ~ 1.6 $/m^3 which is due to the decrease in the operating cost of the MVC unit. Further increase in the number of effects between 2 to 6 brings little increase in the η_{II}, especially for the PCF configuration. In addition, there is no significant change in the SPC for both feed configurations. On the other hand, the value of TWP price keeps increasing with the increase in N which is due to the continuous increase in the required heat transfer area (capital cost). Increasing N beyond 6 leads to an increase in the SPC and η_{II} for both the FF and PCF configurations at a given production capacity. This is attributed to the large decrease in the volumetric vapor flow rate through the MVC unit which may not be sufficient to generate the required amount of vapor in the first effect. This low amount of vapor routed in the MVC unit from the last effect has to be compensated partially by adding extra energy E_{SH} by superheating the vapor through the MVC unit. Increasing the number of effects from 2 to 10 causes an increase in the TWP by 16% and 63% for the PCF and FF configurations, respectively. The use of more than 2 effects in the MED-MVC system does not improve the SPC compared to conventional MED. The main reason for not using multiple effects beyond 6 in MVC systems is the practical limitation of the displacement volume of the commercially available compressors [62]. In the literature, there is no report for the actual installation of MED-MVC systems with more than 6 effects [9].

Another critical factor addressed in the current study is the effect of the compressor pressure head on the plant operating performance and economic parameters. Fig. 9 shows the effect of variation of the compressed vapor temperature (55 to 110^{o}C) on the SPC, η_{II} and TWP for a 4-effect MED-MVC system operating in a PCF configuration. At the low-temperature difference between the compressed vapor and the last effect vapor, the compression ratio decreases which decreases the SPC power consumed through the compression process and the highest η_{II} is obtained. Although the required specific heat transfer area is large, the TWP shows the lowest value (1.6 $/m^3) for steam temperature around 60^{o}C. On the other hand, at the high-temperature difference, the specific heat transfer area decreases but the TWP continues to increase significantly. This is attributed to the increase in the operating cost of the MVC unit with the

increase of the SPC. Lowering the steam temperature from 110 to 55°C results in 100% increase in the η_{II} , and 20 and 40% decrease in the SPC and TWP, respectively. Finally, it should be mentioned that the values of SPC and TWP at the operating temperatures simulated are consistent with the data available in the literature [22, 33, 46, 58, 61].

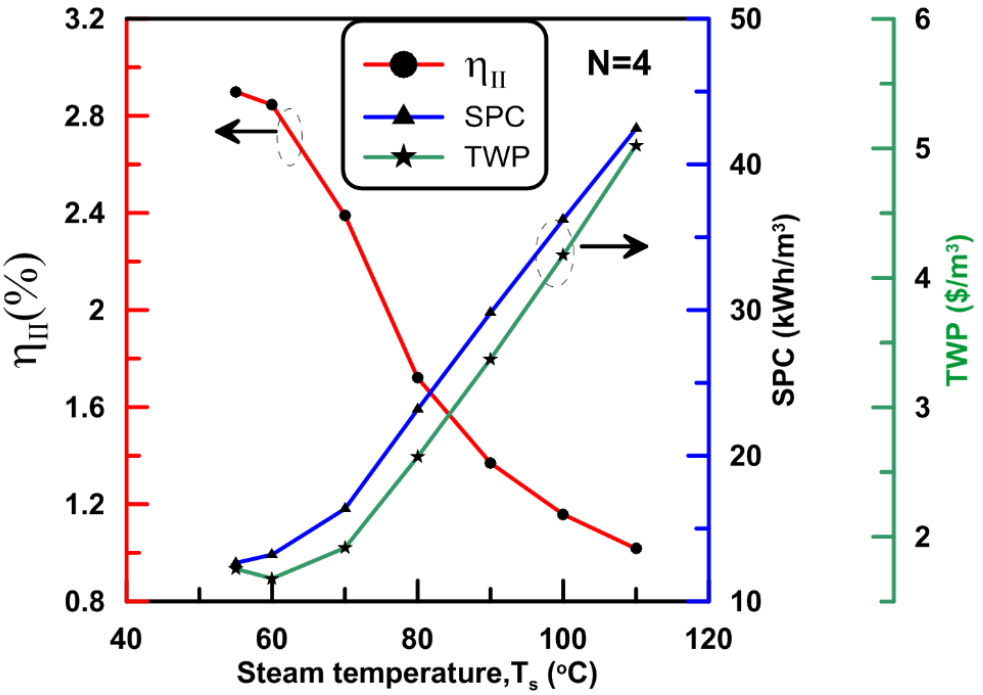

Fig. 9 Effect of steam temperature on SPC, η_{II} and TWP for PCF feed configuration.

Conclusions

In the current study a new formulation for the steady-state thermodynamic model of MED-MVC desalination systems operating in different feed configurations has been presented. The effects of using different feed configurations for a MED-MVC desalination system on the total water price and plant performance are investigated. The calculated performance ratio (PR) is 2.89, 3.19, 3.0 and 3.33 for BF, FF, PF and PCF, respectively. Of the four configurations, the FF configuration yields the lowest specific power consumption (13.7 kWh/m^3), followed by the PCF configuration. The study reveals that the exergy destructions in the MVC unit (~35 to 50%) and evaporator units (~34 to 50%) represent the highest share of the total exergy destruction in the system. Other components, such as the brine and distillate feed heaters, have much lower shares in the exergy destruction which range between 7.6 to 10.9 % for all

configurations. The second law efficiency is the highest for the PCF configuration (2.9%), while the BF has the lowest value (2.38%). The fixed cost for the BF configuration is the highest compared to the other configurations.

Results from the present economic models show that the most expensive (highest investment cost) components are the evaporator units. For the PF and FF configurations, the low values of the variable f_k for the MVC unit, evaporator units and the two preheaters show that the costs associated with these components are dominated by exergy destruction with the remaining costs determined by the $\dot{Z}_k$value. Reducing the exergy destruction in these units could be cost effective for the entire system even if this would increase the associated capital investment costs. Sensitivity analysis show that the MED-MVC system is superior to the single-effect MVC system, but there is a limit on the number of effects N that can be implemented. Increasing the number of effects from 2 to 6 results in no significant increase in the SPC or η_{II} for both the PF and FF configurations. On the contrary, the value of TWP increases by 15 and 63% as the number of effects increases from 2 to 10 for the FF and PCF configurations, respectively. Also, lowering the steam temperature supplied by the MVC unit from 110 to 55^{o}C results in 100% increase in the η_{II} , and 20 and 40 % decrease in the SPC and TWP, respectively. By using average values for the economic parameters, different cost models are used to estimate the average total water price for the BF, FF, PF and PCF configurations as 3.0, 1.69, 2.4 and 1.7 \$/m^3, respectively. Changes in the cost index and interest rate have a minimal effect on the total water price. On the other hand, changing the electricity cost has a significant effect on the TWP. The TWP for the PCF configuration could reach 0.92 \$/m^3 if the electricity cost is 0.03 \$/kWh.

Acknowledgments

This work is supported by U.S. Department of Energy (DOE) through the Grant No. DE-SC0015809 and the Egyptian Ministry of Research and Higher Education.

Appendix A.

Table A. 1 Actual installed MED-MVC systems with different industrial applications.

Steam Temp. ^{o}C	Application	Capacity m^3/day	# of effect	SPC kWh/m^3	Energy Source	Location
70	Desalination SW	50	1	14.4	Wind	Gran Canaria, Spain [63]
70	Desalination SW	48	1	16	Wind	Borkum Island, Germany [12]
70	Desalination SW	360	1	16.7	Wind	Rügen Island, Germany [12]
NA	Crystallization WW	28.8	1	58.6	EM	Jiangsu, China [64]
NA	Crystallization WW	48	2	41.5	EM	
63.0	Desalination SW	1600	4	11.25	EM	Porto Empedocle, Italy [65]
72	Desalination SW	3000	3	8.1	EM	Sardinia, Italy [66]
50	Desalination SW	500:4000	1	8:16.5	EM	Installed plant by IDE [33]
60	Desalination WW	0.437	1	120.87	EM	Beihang University, China [67]
106.8		1.7		31.07		
70.5	Desalination SW	100	1	16.578	EM	Kuwait [68]
62.5	Desalination SW	1500	4	11	EM	Flamanville, France [9]
67	Oil recovery	600	1	14.48	EM	Germany [14]
85.1	Oil recovery	1	1	70	EM	São Paulo State, Brazil [69]
65	Desalination SW	50	2	13.6	EM	Trombay, India [54]
105	Desalination SW	1	2	42	EM	National University of Singapore [10]
80	Desalination SW	100	1	11	EM	Copenhagen, Denmark [70]
70	Desalination SW	5	1	14.8	EM	Egypt [11]
105	Desalination SW	50	2	45.6	EM	Tianjin, China [17]
59	Desalination SW	500	1	14.0	EM	Las Palmas, Spain [8]
--	Desalination SW	1.8	1	33.29	EM	Beijing, China [71]
101	Sewage treatment	1.45	1	33.3	EM	Beijing, China [16]
115	Desalination SW	9.6	1	29.4	EM	Beijing, China [72]
63	Desalination SW	500		15.504	Diesel	Palma de Mallorca, Spain [73]
70		2500	1	13.92	engine	

SW: Seawater, WW: Wastewater, EM: Electrical motor

References

[1] H. Lu, J. Wang, T. Wang, N. Wang, Y. Bao, H. Hao, Crystallization techniques in wastewater treatment: An overview of applications, Chemosphere, 173 (2017) 474-484. https://doi.org/10.1016/j.chemosphere.2017.01.070.

[2] L. Weimer, T. Fosberg, L. Musil, Maximizing water recovery/reuse via mechanical vapor-recompression (MVR) evaporation, Environmental Progress & Sustainable Energy, 2 (1983) 246-250. https://doi.org/10.1002/ep.670020410.

[3] Z. Zimerman, Development of large capacity high efficiency mechanical vapor compression (MVC) units, Desalination, 96 (1994) 51-58. https://doi.org/10.1016/0011-9164(94)85156-5.

[4] M. Sharaf, A. Nafey, L. García-Rodríguez, Thermo-economic analysis of solar thermal power cycles assisted MED-VC (multi effect distillation-vapor compression) desalination processes, Energy, 36 (2011) 2753-2764. https://doi.org/10.1016/j.energy.2011.02.015.

[5] Y.M. El-Sayed, Thermoeconomics of some options of large mechanical vapor-compression units, Desalination, 125 (1999) 251-257. https://doi.org/10.1016/S0011-9164(99)00146-0.

[6] V.C. Onishi, A. Carrero-Parreño, J.A. Reyes-Labarta, R. Ruiz-Femenia, R. Salcedo-Díaz, E.S. Fraga, J.A. Caballero, Shale gas flowback water desalination: Single vs multiple-effect evaporation with vapor recompression cycle and thermal integration, Desalination, 404 (2017) 230-248. https://doi.org/10.1016/j.desal.2016.11.003.

[7] M. Ahmadi, E. Baniasadi, H. Ahmadikia, Process modeling and performance analysis of a productive water recovery system, Applied Thermal Engineering, 112 (2017) 100-110. https://doi.org/10.1016/j.applthermaleng.2016.10.067.

[8] J. Veza, Mechanical vapour compression desalination plants—A case study, Desalination, 101 (1995) 1-10. https://doi.org/10.1016/0011-9164(95)00002-J.

[9] M. Lucas, B. Tabourier, The mechanical vapour compression process applied to seawater desalination: a 1,500 ton/day unit installed in the nuclear power plant of Flamanville, France, Desalination, 52 (1985) 123-133. https://doi.org/10.1016/0011-9164(85)85003-7.

[10] R. Bahar, M.N.A. Hawlader, L.S. Woei, Performance evaluation of a mechanical vapor compression desalination system, Desalination, 166 (2004) 123-127. https://doi.org/10.1016/j.desal.2004.06.066.

[11] N.H. Aly, A.K. El-Figi, Mechanical vapor compression desalination systems—a case study, Desalination, 158 (2003) 143-150. https://doi.org/10.1016/S0011-9164(03)00444-2.

[12] U. Plantikow, Wind-powered MVC seawater desalination—operational results, Desalination, 122 (1999) 291-299. https://doi.org/10.1016/S0011-9164(99)00049-1.

[13] D.L. Shaffer, L.H. Arias Chavez, M. Ben-Sasson, S. Romero-Vargas Castrillón, N.Y. Yip, M. Elimelech, Desalination and reuse of high-salinity shale gas produced water: drivers, technologies, and future directions, Environmental science & technology, 47 (2013) 9569-9583. https://doi.org/10.1021/es401966e.

[14] A. Koren, N. Nadav, Mechanical vapour compression to treat oil field produced water, Desalination, 98 (1994) 41-48. https://doi.org/10.1016/0011-9164(94)00130-8.

[15] D. Han, W. He, C. Yue, W. Pu, Study on desalination of zero-emission system based on mechanical vapor compression, Applied Energy, 185 (2017) 1490-1496. https://doi.org/10.1016/j.apenergy.2015.12.061.

[16] H. Wu, Y. Li, J. Chen, Research on an evaporator-condenser-separated mechanical vapor compression system, Desalination, 324 (2013) 65-71. https://doi.org/10.1016/j.desal.2013.06.004.

[17] J. Shen, Z. Xing, K. Zhang, Z. He, X. Wang, Development of a water-injected twin-screw compressor for mechanical vapor compression desalination systems, Applied Thermal Engineering, 95 (2016) 125-135. https://doi.org/10.1016/j.applthermaleng.2015.11.057.

[18] J. Shen, Z. Xing, X. Wang, Z. He, Analysis of a single-effect mechanical vapor compression desalination system using water injected twin screw compressors, Desalination, 333 (2014) 146-153. https://doi.org/10.1016/j.desal.2013.10.014.

[19] H.S. Aybar, Analysis of a mechanical vapor compression desalination system, Desalination, 142 (2002) 181-186. https://doi.org/10.1016/S0011-9164(01)00437-4.

[20] D. Aussenac, M. Enjalbert, S. Domenech, Mathematical model of a mechanical-vapor compression evaporator. Application to the production of freshwater by seawater desalination: Part II—Numerical exploitation, Desalination, 49 (1984) 111-139. https://doi.org/10.1016/0011-9164(84)85026-2.

[21] G. Aly, Computer simulations of multiple-effect FFE-VC systems for water desalination, Desalination, 45 (1983) 119-131. https://doi.org/10.1016/0011-9164(83)87209-9.

[22] A. Nafey, H. Fath, A. Mabrouk, Thermoeconomic design of a multi-effect evaporation mechanical vapor compression (MEE–MVC) desalination process, Desalination, 230 (2008) 1-15. https://doi.org/10.1016/j.desal.2007.08.021.

[23] C. Fernández-López, A. Viedma, R. Herrero, A. Kaiser, Seawater integrated desalination plant without brine discharge and powered by renewable energy systems, Desalination, 235 (2009) 179-198. https://doi.org/10.1016/j.desal.2007.10.041.

[24] A. Helal, S. Al-Malek, Design of a solar-assisted mechanical vapor compression (MVC) desalination unit for remote areas in the UAE, Desalination, 197 (2006) 273-300. https://doi.org/10.1016/j.desal.2006.01.021.

[25] C.R. Henderson, J.F. Manwell, J.G. McGowan, A wind/diesel hybrid system with desalination for Star Island, NH: feasibility study results, Desalination, 237 (2009) 318-329. https://doi.org/10.1016/j.desal.2005.07.054.

[26] D. Zejli, A. Ouammi, R. Sacile, H. Dagdougui, A. Elmidaoui, An optimization model for a mechanical vapor compression desalination plant driven by a wind/PV hybrid system, Applied energy, 88 (2011) 4042-4054. https://doi.org/10.1016/j.apenergy.2011.04.031.

[27] S.H. Mounir, M. Feidt, C. Vasse, Thermoeconomic study of a system for pollutant concentration with mechanical vapour compression, Applied thermal engineering, 25 (2005) 473-484. https://doi.org/10.1016/j.applthermaleng.2004.05.011.

[28] M.H. Sharqawy, S.M. Zubair, On exergy calculations of seawater with applications in desalination systems, International Journal of Thermal Sciences, 50 (2011) 187-196. https://doi.org/10.1016/j.ijthermalsci.2010.09.013.

[29] F.N. Alasfour, H.K. Abdulrahim, The effect of stage temperature drop on MVC thermal performance, Desalination, 265 (2011) 213-221. https://doi.org/10.1016/j.desal.2010.07.054.

[30] M.A. Jamil, S.M. Zubair, Design and analysis of a forward feed multi-effect mechanical vapor compression desalination system: An exergo-economic approach, Energy, 140 (2017) 1107-1120. https://doi.org/10.1016/j.energy.2017.08.053.

[31] K.H. Mistry, R.K. McGovern, G.P. Thiel, E.K. Summers, S.M. Zubair, J.H. Lienhard, Entropy generation analysis of desalination technologies, Entropy, 13 (2011) 1829-1864. https://doi.org/10.3390/e13101829.

[32] H. Wu, Y. Li, J. Chen, Analysis of an evaporator-condenser-separated mechanical vapor compression system, Journal of Thermal Science, 22 (2013) 152-158. https://doi.org/10.1007/s11630-013-0606-1.

[33] R. Matz, U. Fisher, A comparison of the relative economics of sea water desalination by vapour compression and reverse osmosis for small to medium capacity plants, Desalination, 36 (1981) 137-151. https://doi.org/10.1016/S0011-9164(00)88637-3.

[34] F. Al-Juwayhel, H. El-Dessouky, H. Ettouney, Analysis of single-effect evaporator desalination systems combined with vapor compression heat pumps, Desalination, 114 (1997) 253-275. https://doi.org/10.1016/S0011-9164(98)00017-4.

[35] H.T. El-Dessouky, H.M. Ettouney, Plastic/compact heat exchangers for single-effect desalination systems, Desalination, 122 (1999) 271-289. https://doi.org/10.1016/S0011-9164(99)00048-X.

[36] V.G. Gude, Energy storage for desalination processes powered by renewable energy and waste heat sources, Applied Energy, 137 (2015) 877-898. https://doi.org/10.1016/j.apenergy.2014.06.061.

[37] S. Mussati, N. Scenna, E. Tarifa, S. Franco, J. Hernandez, Optimization of the mechanical vapor compression (MVC) desalination process using mathematical programming, Desalination and Water Treatment, 5 (2009) 124-131. https://doi.org/10.5004/dwt.2009.572.

[38] M.L. Elsayed, O. Mesalhy, R.H. Mohammed, L.C. Chow, Effect of disturbances on MED-TVC plant characteristics: Dynamic modeling and simulation, Desalination, 443 (2018) 99-109. https://doi.org/10.1016/j.desal.2018.05.021.

[39] H.T. El-Dessouky, H.M. Ettouney, Fundamentals of salt water desalination, Elsevier, 2002.

[40] M.L. Elsayed, O. Mesalhy, R.H. Mohammed, L.C. Chow, Effect of input parameters intensity and duration on dynamic performance of MED-TVC plant, Applied Thermal Engineering, 137 (2018) 475-486. https://doi.org/10.1016/j.applthermaleng.2018.03.106.

[41] M.W. Shahzad, K. Thu, Y.-d. Kim, K.C. Ng, An experimental investigation on MEDAD hybrid desalination cycle, Applied Energy, 148 (2015) 273-281. https://doi.org/10.1016/j.apenergy.2015.03.062.

[42] R. Buonopane, R. Troupe, J. Morgan, Heat transfer design method for plate heat exchangers, Chemical Engineering Progress, 59 (1963) 57-61.

[43] H.-S. Choi, T.-J. Lee, Y.-G. Kim, S.-L. Song, Performance improvement of multiple-effect distiller with thermal vapor compression system by exergy analysis, Desalination, 182 (2005) 239-249. https://doi.org/10.1016/j.desal.2005.03.018.

[44] K. Ansari, H. Sayyaadi, M. Amidpour, Thermoeconomic optimization of a hybrid pressurized water reactor (PWR) power plant coupled to a multi effect distillation desalination system with thermo-vapor compressor (MED-TVC), Energy, 35 (2010) 1981-1996. https://doi.org/10.1016/j.energy.2010.01.013.

[45] M.M. El-Halwagi, Sustainable design through process integration: fundamentals and applications to industrial pollution prevention, resource conservation, and profitability enhancement, Butterworth-Heinemann, 2017.

[46] N. Lukic, L. Diezel, A. Fröba, A. Leipertz, Economical aspects of the improvement of a mechanical vapour compression desalination plant by dropwise condensation, Desalination, 264 (2010) 173-178. https://doi.org/10.1016/j.desal.2010.07.023.

[47] W. El-Mudir, M. El-Bousiffi, S. Al-Hengari, Performance evaluation of a small size TVC desalination plant, Desalination, 165 (2004) 269-279. https://doi.org/10.1016/j.desal.2004.06.031.

[48] Y. El-Sayed, Designing desalination systems for higher productivity, Desalination, 134 (2001) 129-158. https://doi.org/10.1016/S0011-9164(01)00122-9.

[49] A. Malek, M. Hawlader, J. Ho, Design and economics of RO seawater desalination, Desalination, 105 (1996) 245-261. https://doi.org/10.1016/0011-9164(96)00081-1.

[50] H. Sayyaadi, A. Saffari, Thermoeconomic optimization of multi effect distillation desalination systems, Applied Energy, 87 (2010) 1122-1133. https://doi.org/10.1016/j.apenergy.2009.05.023.

[51] S. Usón, A. Valero, A. Agudelo, Thermoeconomics and industrial symbiosis. Effect of by-product integration in cost assessment, Energy, 45 (2012) 43-51. https://doi.org/10.1016/j.energy.2012.04.016.

[52] A. Bejan, G. Tsatsaronis, Thermal design and optimization, John Wiley & Sons, 1996.

[53] Y. Wang, N. Lior, Thermoeconomic analysis of a low-temperature multi-effect thermal desalination system coupled with an absorption heat pump, Energy, 36 (2011) 3878-3887. https://doi.org/10.1016/j.energy.2010.09.028.

[54] G. Kishore, S. Nisan, S. Dardou, A. Adak, V. Srivastava, P. Tewari, Development of a dynamic simulator (INFMED) for the MED/VC plant, Desalination and Water Treatment, 21 (2010) 364-374. https://doi.org/10.5004/dwt.2010.1752.

[55] M.A. Rosen, A concise review of exergy-based economic methods, Proc. 3rd IASME/WSEAS Int. Conf. on Energy & Environment, (2008) 136-144.

[56] Y. Cerci, The minimum work requirement for distillation processes, Exergy, An International Journal, 2 (2002) 15-23. https://doi.org/10.1016/S1164-0235(01)00036-X.

[57] F. Hafdhi, T. Khir, A.B. Yahia, A.B. Brahim, Exergoeconomic optimization of a double effect desalination unit used in an industrial steam power plant, Desalination, 438 (2018) 63-82. https://doi.org/10.1016/j.desal.2018.03.020.

[58] A.A. Mabrouk, A. Nafey, H. Fath, Thermoeconomic analysis of some existing desalination processes, Desalination, 205 (2007) 354-373. https://doi.org/10.1016/j.desal.2006.02.059.

[59] M.L. Elsayed, O. Mesalhy, R.H. Mohammed, L.C. Chow, Exergy and thermo-economic analysis for MED-TVC desalination systems, Desalination, 447 (2018) 29-42. https://doi.org/10.1016/j.desal.2018.06.008.

[60] M.L. Elsayed, O. Mesalhy, R.H. Mohammed, L.C. Chow, Transient performance of MED processes with different feed configurations, Desalination, 438 (2018) 37-53. https://doi.org/10.1016/j.desal.2018.03.016.

[61] S. Frioui, R. Oumeddour, Investment and production costs of desalination plants by semi-empirical method, Desalination, 223 (2008) 457-463. https://doi.org/10.1016/j.desal.2007.01.180.

[62] M. Darwish, Thermal analysis of vapor compression desalination system, Desalination, 69 (1988) 275-295. https://doi.org/10.1016/0011-9164(88)80030-4.

[63] J. Carta, J. Gonzalez, V. Subiela, The SDAWES project: an ambitious R&D prototype for wind-powered desalination, Desalination, 161 (2004) 33-48. https://doi.org/10.1016/S0011-9164(04)90038-0.

[64] L. Liang, D. Han, R. Ma, T. Peng, Treatment of high-concentration wastewater using double-effect mechanical vapor recompression, Desalination, 314 (2013) 139-146. https://doi.org/10.1016/j.desal.2013.01.016.

[65] L. Rizzuti, H.M. Ettouney, A. Cipollina, Solar desalination for the 21st century: a review of modern technologies and researches on desalination coupled to renewable energies, Springer Science & Business Media, 2007.

[66] G. Kronenberg, F. Lokiec, Low-temperature distillation processes in single-and dual-purpose plants, Desalination, 136 (2001) 189-197. https://doi.org/10.1016/S0011-9164(01)00181-3.

[67] Y. Li, H. Wu, X. Liang, C. Rong, H. Chen, Experimental study of waste concentration by mechanical vapor compression technology, Desalination, 361 (2015) 46-52. https://doi.org/10.1016/j.desal.2015.01.036.

[68] M. Darwish, M.A. Jawad, G. Aly, Comparison between small capacity mechanical vapor compression (MVC) and reverse osmosis (RO) desalting plants, Desalination, 78 (1990) 313-326. https://doi.org/10.1016/0011-9164(90)80052-D.

[69] B.G. Andrade, V.T. Andrade, B.R. Costa, J.C. Campos, M. Dezotti, Distillation of oil field produced water for reuse on irrigation water: evaluation of pollutants removal and ecotoxicity, Journal of Water Reuse and Desalination, 1 (2011) 224-236. https://doi.org/10.2166/wrd.2011.044.

[70] N.-E. Clausen, Development of a plate evaporator/condenser for the mechanical vapour compression process, Desalination, 81 (1991) 399-406. https://doi.org/10.1016/0011-9164(91)85072-3.

[71] W.K. Pang, L.W. Yang, Z.T. Zhang, Operation Characteristic of a Mechanical Vapor Recompression Heat Pump Driven by a Centrifugal Fan, Advanced Materials Research, 732 (2013) 165-171. https://doi.org/10.4028/www.scientific.net/AMR.732-733.165.

[72] J. Yang, C. Zhang, Z. Zhang, L. Yang, W. Lin, Study on mechanical vapor recompression system with wet compression single screw compressor, Applied Thermal Engineering, 103 (2016) 205-211. https://doi.org/10.1016/j.applthermaleng.2016.04.053.

[73] W. Bulang, Desalination by vapor compression, Desalination, 38 (1981) 85-97. https://doi.org/10.1016/S0011-9164(00)86051-8.

Nomenclature

Latin

A	Heat transfer area m^2
A_f	amortization factor, (1/year)
BPE	Boiling point elevation °C
$\dot{C}_F$	Fuel cost rate ($/h)
$\dot{C}_F$	Product cost rate ($/h)
$\dot{E}$	Exergy, kW
h	Enthalpy of saturated water, kJ/kg
h_{fg}	Latent heat of evaporation, kJ/kg
m	Mass flow rate kg/s
P	Pressure, kPa
PR	Performance ratio
ppt	Part per thousand, g/kg
Q	Heat transfer rate, kW
T	Temperature, ^oC
T_{feed}	Seawater feed temperature, ^oC
$T_{hin,d}$	Distillate mix temperature, ^oC
TBT	Top brine temperature, ^oC
U	Overall heat transfer coefficient, $W/m^2.{}^oC$
$\dot{W}$	Work, kW
X	Salinity, ppt
Z	Component purchasing cost, $

Greek

ρ	density, kg m^{-3}
ε	error criterion
ϵ	Exergetic efficiency
λ	Latent heat of evaporation, kJ/kg
η	Second law efficiency
μ	Chemical potential, kJ/kg
δ	Difference

Subscripts:

cw	Cooling water
D	destruction
E	Evaporator/effect
f	feed
i	Effect number
k	component
L	liquid
n	Last effect
o	out
s	steam
sat	Saturation
SH	superheat
sw	seawater
v	vapor